AD-A123 682 OPTICAL TIME DOMAIN REFLECTOMETRY FIBER STUDIES(U) 1/1
HUGHES RESEARCH LABS MALIBU CA M D ROURKE ET AL.
NOV 82 RADC-TR-82-281 F19628-79-C-0172

UNCLASSIFIED F/G 20/6 NL

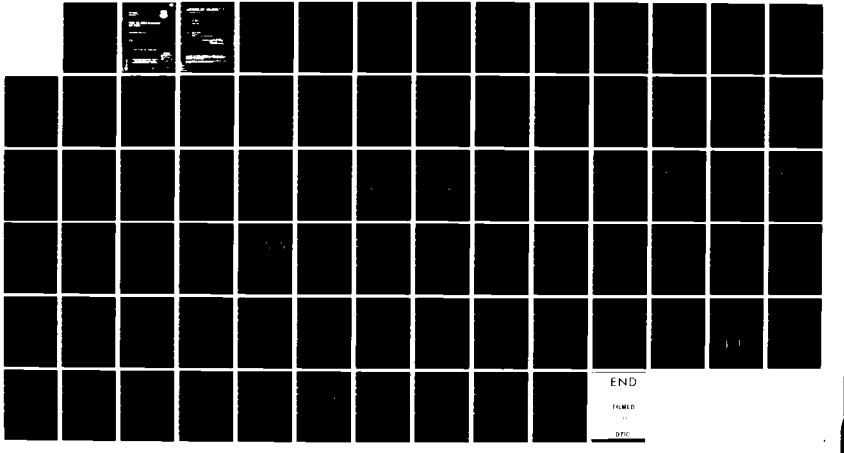

END

FILMED

DTIC

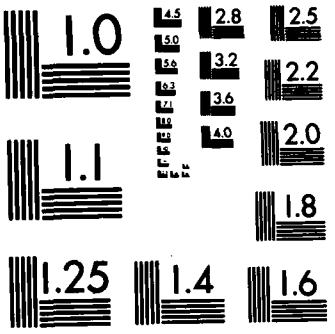

MICROCOPY RESOLUTION TEST CHART
NATIONAL BUREAU OF STANDARDS-1963-A

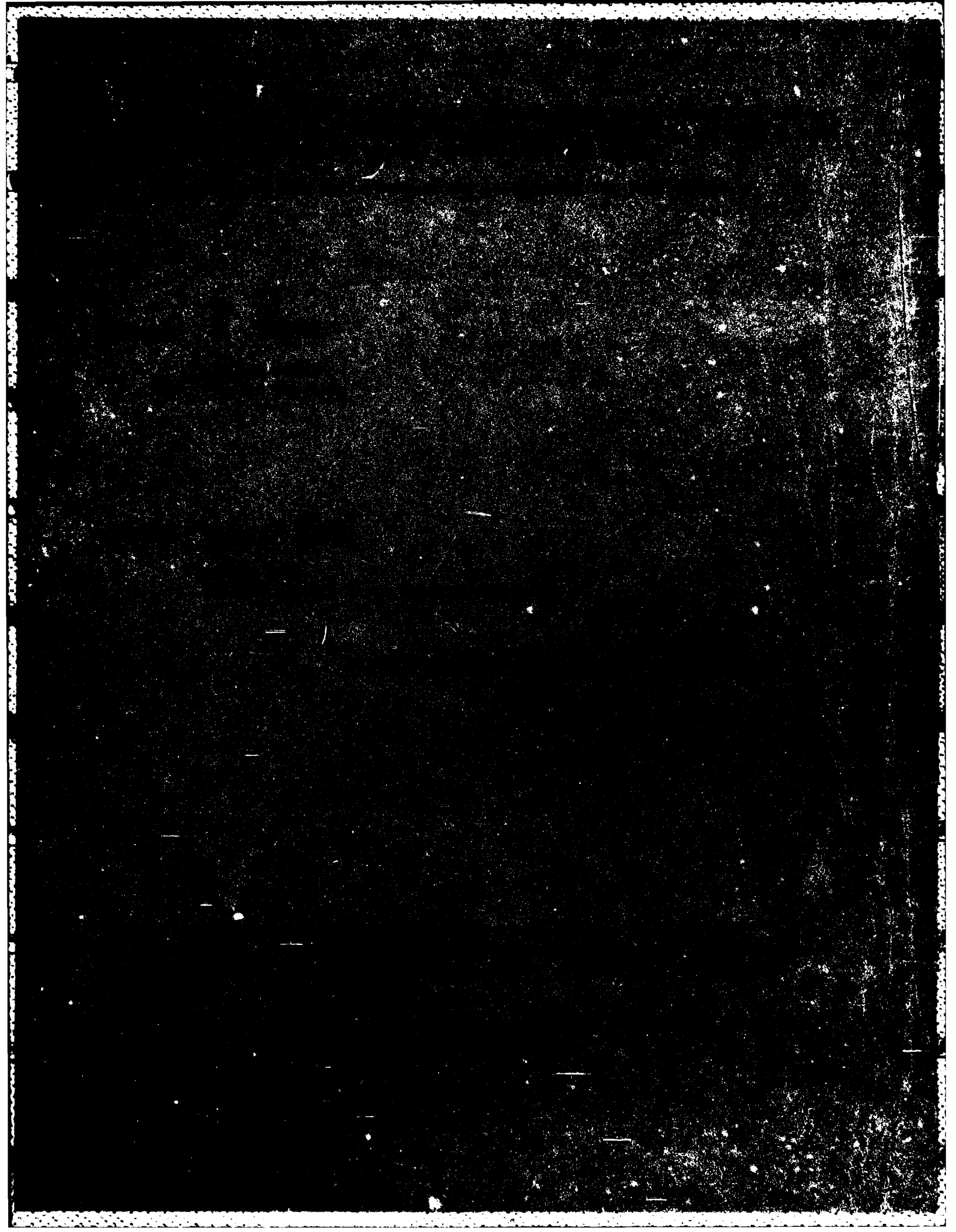

UNCLASSIFIED

SECURITY CLASSIFICATION OF THIS PAGE (When Data Entered)

REPORT DOCUMENTATION PAGE		READ INSTRUCTIONS BEFORE COMPLETING FORM
1. REPORT NUMBER RADC-TR-82-281	2. GOVT ACCESSION NO.	3. RECIPIENT'S CATALOG NUMBER
4. TITLE (and Subtitle) OPTICAL TIME DOMAIN REFLECTOMETRY FIBER STUDIES		5. TYPE OF REPORT & PERIOD COVERED Final Technical Report November 1982 6. PERFORMING ORG. REPORT NUMBER N/A
7. AUTHOR(s) M.D. Rourke H.W. Yen		8. CONTRACT OR GRANT NUMBER(s) F19628-79-C-0172
9. PERFORMING ORGANIZATION NAME AND ADDRESS Hughes Research Laboratories 3011 Malibu Canyon Road Malibu CA 90265		10. PROGRAM ELEMENT, PROJECT, TASK AREA & WORK UNIT NUMBERS 33401G 78200225
11. CONTROLLING OFFICE NAME AND ADDRESS Rome Air Development Center (ESOC) Hanscom AFB MA 01731		12. REPORT DATE November 1982 13. NUMBER OF PAGES 86
14. MONITORING AGENCY NAME & ADDRESS(if different from Controlling Office) Same		15. SECURITY CLASS. (of this report) UNCLASSIFIED 15a. DECLASSIFICATION/DOWNGRADING SCHEDULE N/A

16. DISTRIBUTION STATEMENT (of this Report)

Approved for public release; distribution unlimited

17. DISTRIBUTION STATEMENT (of the abstract entered in Block 20, if different from Report)

Same

18. SUPPLEMENTARY NOTES

RADC Project Engineer: Richard Payne (ESOC)

19. KEY WORDS (Continue on reverse side if necessary and identify by block number)

Optical time domain reflectometry (OTDR)
Secure communication
OTDR signature
Intrusions
Microbends
Optical fiber
Perturbations in fiber
Sensitivity of OTDR

20. ABSTRACT (Continue on reverse side if necessary and identify by block number)

The wideband frequency capability of optical fibers, the development of very low loss optical fibers (< 1 dB/km) and the rapid development of associated optical circuit elements are expected to result in widespread use of optical fiber communication systems in the near future. However, hostile intrusion into these fiber links requires immediate attention and studies, along with a method for detecting these intrusions before hard standards for secure fiber links can be set.

DD FORM 1 JAN 73 1473 EDITION OF 1 NOV 65 IS OBSOLETE

UNCLASSIFIED

SECURITY CLASSIFICATION OF THIS PAGE (When Data Entered)

Optical time domain reflectometry (OTDR) has been suggested as a tool for detecting intrusions in a fiber. This is based on the knowledge that the OTDR is very sensitive in locating and measuring fiber perturbations, including loops, bubbles, and sinusoidal perturbations of optic axis and core diameter.

The program goal is to develop the OTDR for intrusion monitoring and to establish its ultimate performance limits. An additional objective is to identify and catalog OTDR signatures of different potential intrusions.

Theoretical considerations indicated that maximum perturbation sensitivity of the OTDR is achieved by increasing the source power until the threshold for stimulated effects is reached. This maximizes sensitivity regardless of the relative shapes of the probe pulse and the perturbation response. Tailoring the probe pulse shape to be a matched filter for the perturbation results in a further increase in sensitivity at the cost of greatly increased complexity in the source.

Several characteristics of perturbation signatures have been found. Perturbations which are much smaller in spatial extent than the probe pulse are characterized by the shape of the probe pulse. If the probe pulse width is much smaller than the spatial extent of the perturbation, the OTDR response is the impulse response of the perturbation.

Experiments on splices indicate that it is very difficult to splice together two waveguides so perfectly that the OTDR is unable to detect the splice. In every observed case, an insertion loss was measured and conversion of bound mode power to leaky modes was observed.

Experiments on measuring the excess loss of a single fiber loop indicated that the OTDR technique is capable of detecting loops as large as 8-cm in diameter. Larger diameter loops can be located if the system signal-to-noise ratio is improved.

Large as well as small amplitude microbends in a step-index waveguide can easily be located and measured with the OTDR.

A single microbend less than 10 μm in amplitude and a periodic microbend (~40 periods) of amplitude less than 2 μm were detectable with a computerized OTDR test set.

TABLE OF CONTENTS

LIST OF ILLUSTRATIONS

SECTION 1

INTRODUCTION AND SUMMARY

Wideband communications systems of the near future will use optical fibers as the transmission medium instead of conventional conducting metal waveguides. The limiting factors of conventional systems are high attenuation, high costs, and large size and weight. By contrast, the wideband frequency capability of optical fibers, the development of very low loss optical fibers (<1 dB/km), the rapid development of associated optical circuit elements (such as connectors, optical sources, detectors, optical couplers, switches, and multiplexers), and the promise of eventual low costs for these key elements are expected to result in widespread use of optical fiber communication systems. However, hostile intrusion into these optical communication links, particularly into DOD links, will require immediate attention and studies, along with a method for detecting these intrusions, before hard standards for secure fiber communication links can be set.

Recently, a new concept for detecting intrusions using an optical time domain reflectometer (OTDR) has been suggested. This suggestion is based on the knowledge that the OTDR is a sensitive tool for locating and measuring fiber perturbations including loops, bubbles, and sinusoidal perturbations of optic axis and core diameter.

The great advantage of OTDR monitoring is that the intrusion point can be quickly determined and corrective action applied at that point. Although the technique currently employed for monitoring intrusion — by monitoring the change in transmitted light intensity or modal characteristics of the light transmitted from station to station — is adequate for detecting an intrusion, it does not appear capable of providing information that can be used to localize the point of intrusion. Thus, OTDR monitoring provides an attractive complement to transmission monitoring.

There are various methods for tapping power from an optical fiber communication system (as there are from copper communication links). Periodic deformation of the fiber, microbending of fibers, proximity coupling, etc. are methods suitable for tapping power from an optical fiber. These intrusion methods result in power loss from the fiber and are detectable with the OTDR. In addition to localizing the position of intrusion, it is desirable to characterize

these intrusions with "signatures" using the OTDR. It may be possible to relate different types of intrusions to different signatures. It is one of the goals of this research program to determine whether a high-sensitivity OTDR can resolve signatures characteristic of the intrusion.

An additional potential advantage of determining intrusion signatures is to compare these signatures with those occurring from environmental events affecting the fiber. Environmental events include random or steady winds, rapid temperature changes resulting in the fiber rubbing in its cabling, strain-induced loss in the fiber, and microbending losses. The resulting fiber losses may cause frequent false intrusion alarms if conventional monitoring is used alone and could result in substantial link down-time. If the signatures of environmental events are found to be considerably different from those of real intrusions, the down-time of the communication link can be decreased significantly by shutting down the link only when an intrusion signature appears.

The purpose of this program is to develop the OTDR for intrusion monitoring and to establish its ultimate performance limits. A primary objective of this program is to determine both the ultimate resolution and the ultimate sensitivity of the OTDR. An additional objective of this effort is to identify and catalog OTDR "signatures" of different potential intrusions. Since each type of potential intrusion affects the bound modes of the fiber in a different way, the OTDR characterization of each intrusion is unique. Consequently, a catalog of intrusion signatures can be made.

Major accomplishments of this program are listed below:

- Theoretical considerations of the maximum sensitivity of the OTDR technique to the presence of perturbations.
- Modifications and improvements of the OTDR test set to facilitate measurements of perturbations.
- Detection of the presence of a single loop in an optical fiber.
- Detection of the presence of fiber splices and microbend transducers.

- Measurement of the insertion loss of a single microbeand.
- Measurements of the diameter variations of a fiber and its correlation to the OTDR signature.
- Investigation of the effects of a periodic microbend transducer on fiber loss.

SECTION 2

REVIEW OF THE OTDR TECHNIQUE

The method of measuring waveguide attenuation with the optical time domain reflectometer (OTDR) is often referred to as the backscattering method. It measures the time rate of change of light Rayleigh backscattered from an optical pulse propagating along a waveguide. The rate of change is fitted to an exponential, $\exp(-2\alpha x)$, where

$$x = \frac{ct}{n} , \tag{1}$$

and c/n is the group velocity. Attenuation A is defined by

$$A = 4.34\ \alpha x \quad . \tag{2}$$

If the distance, x, is measured in kilometers, attenuation has units of dB/km.

This method has many advantages. In particular, it is unique in providing information on the length dependence of the loss. It is non-destructive, accurate, and highly sensitive to small perturbations. A singular advantage of the technique is that it normally requires access to only one end of the waveguide in order to perform loss measurements. This last feature obviously makes it extremely attractive for use in field installations.

However, the method has two disadvantages: the exact modal distribution of the backscattered power is unknown, and an ambiguity can result when particularly nonuniform waveguides are measured. The ambiguity can be resolved by measuring the waveguide from both ends or by operator interpretation of the data.

The backscattering method permits the measurement of nearly every waveguide parameter.[1] Included in the measurement capabilities are: total attenuation coefficient, scattering coefficient, absorption coefficient, differential mode attenuation, waveguide length, bandwidth, location of defects, faults, connectors, splices, and the effect of the external environment on waveguide properties (including introduction of lossy coatings, strain, and ionizing radiation).

The general experimental arrangement used in the OTDR is shown in Figure 1. Qualitatively, light from a pulsed source is coupled into a waveguide using an optical directional coupler. As the pulse propagates, it encounters a string of absorption and scattering sites which attenuate the beam (see Figures 2(a) and (b); each scattering site* affects the forward-traveling pulse in a unique way. However, each site converts some of the forward traveling pulses into a reverse traveling pulse (Figure 2(c)). That portion of the reverse-traveling pulse which is trapped in the guided modes will be directed back to the directional coupler. As the backscattered pulse propagates, it is again attenuated by the scattering and attenuation sites it encounters. When the resultant signal (Figure 2(d)) reaches the directional coupler (Figure 1) it is routed to a photodetector. The detected signal is amplified and then electronically processed before being displayed and recorded.

A. ANALYSIS OF AN UNPERTURBED WAVEGUIDE

The backscattering method can be analyzed quantitatively by considering a pulse of light propagating along a waveguide. The forward-traveling pulse suffers a position-dependent total attenuation determined by the total attenuation coefficient, γ_{ft}, which, in general, depends upon position and mode group excitation. This coefficient consists of two terms, a scattering term, γ_{fs}, and an absorption term, γ_{fa}.

The scattering term, γ_{fs}, in low-loss waveguides is due predominantly to Rayleigh scattering from two main sources: density fluctuations and concentration fluctuations. Density fluctuations are thermal fluctuations of the glass atoms which are frozen in during waveguide fabrication. The scattering coefficient, γ_{sd}, due to density fluctuations, is related to the isothermal compressibility, β, through the expression,

*Scattering sites are defined here to mean any site which converts a portion of the forward-traveling wave into a reverse-traveling wave. According to this definition, scattering sites include dielectric discontinuities resulting in Fresnel reflection, Rayleigh scattering sites, and point defects that cause reflections.

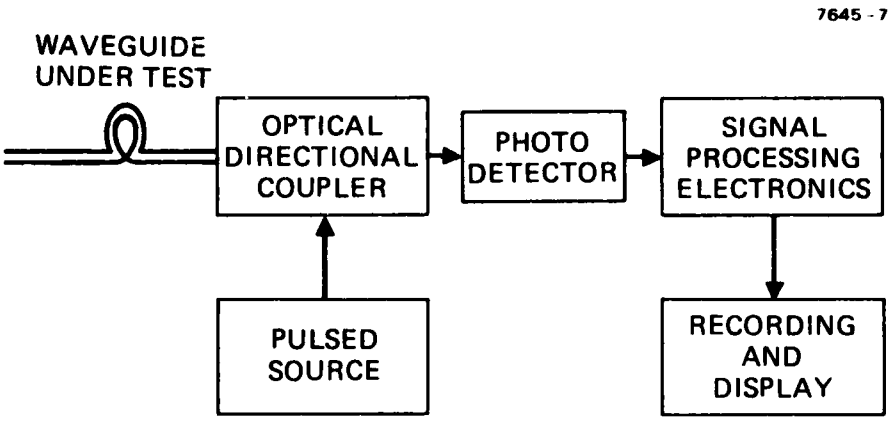

Figure 1.
A block diagram of the OTDR. A pulse of light from the source is coupled into the waveguide under test by an optical directional coupler. The directional coupler also routes the back-scattered signal to a photodetector. The detected signal is amplified and electronically processed before recording and display.

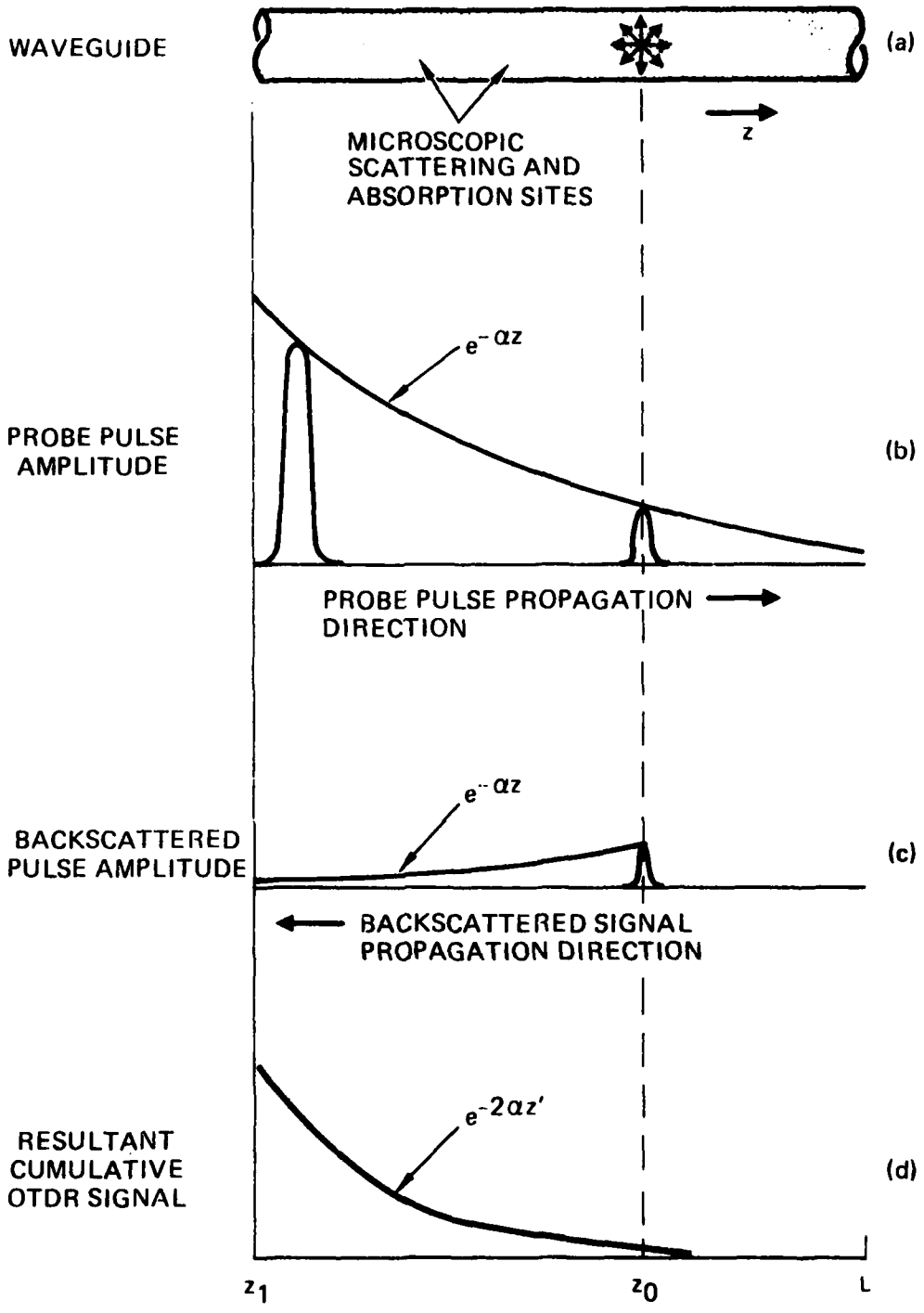

Figure 2.
The backscattering process in a waveguide of length L. The waveguide contains innumerable, randomly-distributed, microscopic scattering and absorption sites, (a). As the probe pulse propagates (b), it is attenuated by these sites. At point z_0 the pulse is backscattered. The backscattered signal is again attenuated by the scattering and absorption sites, (c). The resultant waveform is seen in (d). It has been plotted on a new abscissa, z', to show that this waveform attenuates at twice the rate of the probe pulse if we plot it against the length of the waveguide.

$$\gamma_{sd} = \frac{8\pi^3}{3\lambda^4} (n^2 - 1)\, kT\beta \quad , \tag{3}$$

where n is the refractive index, k is Boltzmann's constant, T is the transition temperature at which the density fluctuations are frozen in, and λ is the wavelength. For fused silica,[2] T is ~800°K and β is ~7 x 10^{-11} m^3/J.

If a glass waveguide is fabricated by introducing an oxide other than SiO_2 to form a region of slightly different index, concentration fluctuations of the dopant oxide will also cause scattering. The scattering coefficient, γ_{sc}, due to concentration fluctuation, is

$$\gamma_{sc} = \frac{16\pi^3}{3\lambda^4} \left(\frac{dn}{dc}\right)^2 \overline{(\Delta c)^2}\ \delta V \quad . \tag{4}$$

where $\overline{(\Delta c)^2}$ is the mean-square concentration fluctuation, and V is the volume over which the concentration fluctuation occurs. For high silica content glass waveguides this scattering mechanism accounts for about 25% of the total scattering.[2] Neglecting any other scattering mechanisms, the total scattering coefficient, γ_{fs}, is

$$\gamma_{fs} = \gamma_{sd} + \gamma_{sc} \quad . \tag{5}$$

The waveguide is characterized by this coefficient and γ_{fa}, the absorption coefficient:

$$\gamma_{ft} = \gamma_{fs} + \gamma_{fa} \quad , \tag{6}$$

where differential modal attenuation is neglected.

The experiment shows that as a pulse propagates down a waveguide the change in power, ΔP, in an incremental distance, Δx, is proportional to the power at that point. Thus,

$$\Delta P_{ft}(x) = -\gamma_{ft}(x) P_{ft}(x) \Delta x \quad . \tag{7}$$

The minus sign indicates that the power decays as the pulse propagates. In the limit as $\Delta x \to 0$, Equation (7) can be rewritten as

$$P_{ft}(z) = P_0 \exp\left[- \int_0^z \gamma_{ft}(x) dx \right] . \tag{8}$$

The backscattered power, P_{bs}, is some fraction, $f(z)$, of the power at position z:

$$P_{bs}(z) = f(z) P_{ft}(z) \quad . \tag{9}$$

As the backscattered signal propagates toward the source, it suffers a position-dependent total attenuation, $\gamma_{bt}(z)$. Consequently, the power backscattered from the pulse at position z that eventually finds its way back to the detector is

$$P(z) = P_0 f(z) \exp\left\{ - \int_0^z \left| \gamma_{ft}(x) + \gamma_{bt}(x) \right| dx \right\} , \tag{10}$$

where P_0 is the initial peak pulse power.

The better waveguides made today exhibit practically no attenuation other than Rayleigh scattering from microscopic density fluctuations frozen in during fabrication.[3] For such a waveguide, the backscattering function is a constant,[4]

$$f(z) = \frac{3}{8} \gamma_s \frac{(NA)^2}{n_o^2} \cdot \frac{\alpha}{\alpha + 1} \quad . \tag{11}$$

Here NA is the numerical aperture, n_0 is the axial refractive index, γ_s is the scattering coefficient (where we assume $\gamma_{fs} = \gamma_{bs} \equiv \gamma_s$), and α is the refractive index profile. This is defined in

$$n^2(r) = \begin{cases} n_0^2 \left[1 - 2\Delta \left(\frac{r}{a}\right)^\alpha\right] & r < a \\ n_2^2 & r > a \end{cases} , \tag{12}$$

where r is the radial coordinate, a is the core radius, n_2 is the refractive index of the cladding, and $\Delta = (n_o^2 - n_2^2)/2n_o^2$ is related to the index difference between core and clad. If the waveguide attenuation is the same for pulses traveling in both directions, the attenuation coefficients are identical; thus

$$\gamma_{ft}(x) = \gamma_{bt}(x) \equiv \gamma_t \tag{13}$$

and

$$\gamma_t = \gamma_s + \gamma_a \ . \tag{14}$$

In this case, Equation (10) reduces to Beer's law:

$$P(z) = \frac{3}{8} \frac{\alpha}{\alpha + 1} \frac{\gamma_s (NA)^2 P_0}{n_0^2} e^{-2\gamma_t z} \ . \tag{15}$$

The OTDR signature of such a commercially available waveguide is shown in Figure 3. The word signature, used to describe the OTDR characterization of a waveguide, emphasizes that each waveguide is unique and exhibits a unique characterization.

Three features are apparent in the signature of Figure 3. First is the Fresnel reflection which occurs at the air-glass interface as the probe pulse enters the waveguide. This reflection is generally undesirable. Next is a

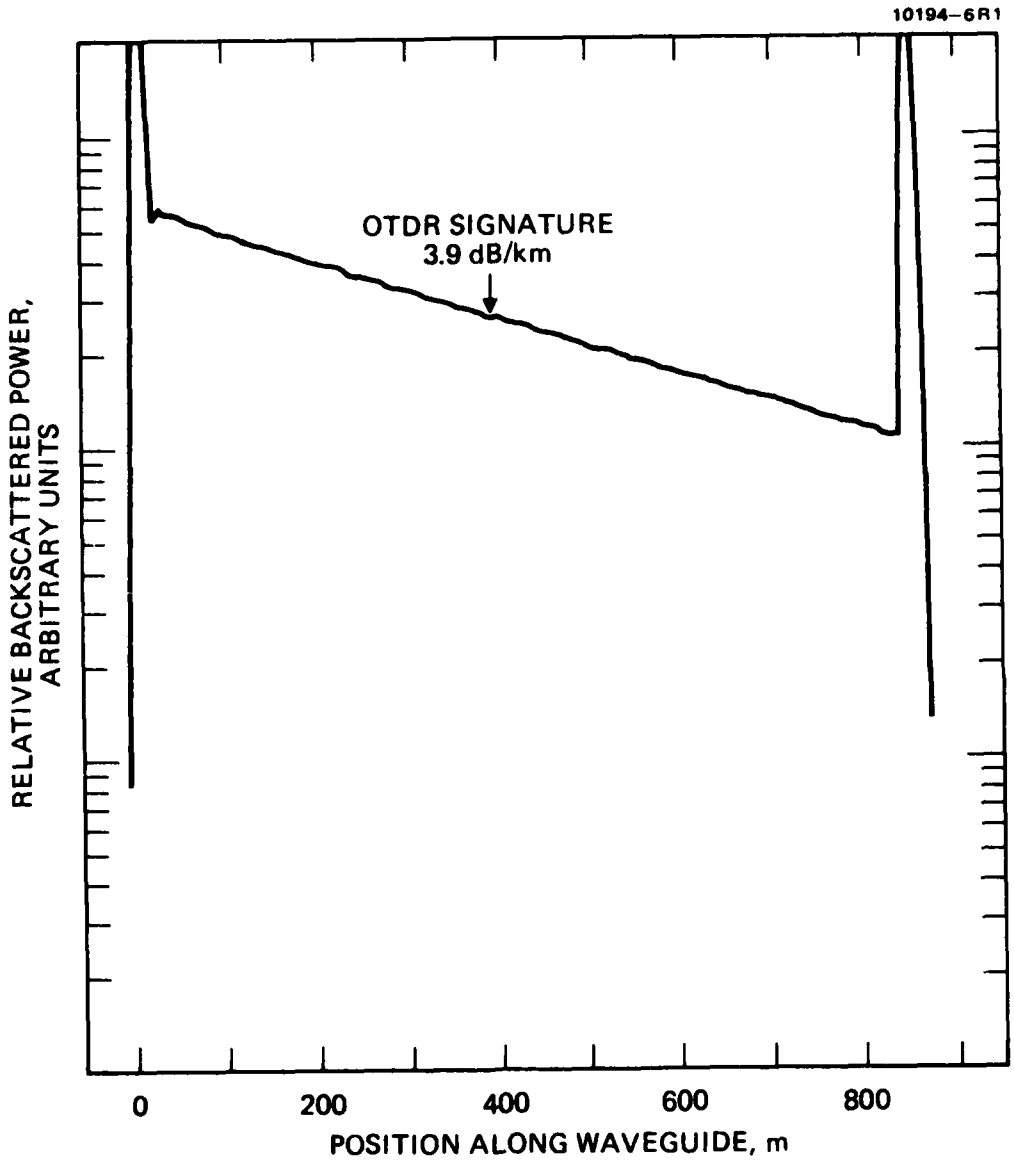

Figure 3.
An OTDR characterization of a low-loss commercially available waveguide. The measurement was made at 0.9 μm. Note the Fresnel reflections which occur at each end of the waveguide and the exponential decay of the Rayleigh scattered light between them.

region of exponential decay of the Rayleigh scattered light. Finally, we see the Fresnel reflection which occurs as the pulse leaves the far end of the waveguide. The amplitude of the reflection from the far end can be used to determine the quality of the cleave, as well as the angle that the cleaved surface makes with the optic axis. The length of the waveguide can be determined by measuring the time delay between the two Fresnel reflections and multiplying by half the group velocity of light in the core.

B. ANALYSIS OF A PERTURBED WAVEGUIDE

The previous discussion assumed that the waveguide was perfect, but most waveguides are imperfect. To determine the OTDR response of an imperfect waveguide, the probe pulse is labeled as Ap(ct-z) and the unperturbed waveguide response as b(z), where A is a constant. Assuming the waveguide response remains linear when a small disturbance d(z) is added, the backscatter power B(t) can be written as

$$B(t) = A\int[b(z) + d(z)]\ p(ct-z)\ dz \quad . \tag{16}$$

Equation (16) is just the sum of convolutions,

$$B = Ab*P + Ad*P \quad , \tag{17}$$

where the symbol (*) denotes the convolution operation. We see from Equation (17) that the OTDR signature consists of two terms: the unperturbed response and the response due to the disturbance.

There are three classes of perturbations of special interest: a very narrow probe pulse, a point defect, and defects where the spatial extent of the probe pulse is approximately equal to that of the defect. Since the operation of convolution is commutative, the first two cases are formally equivalent. In the first case, the probe pulse only samples the perturbation over an incremental distance much less than the width of the perturbation. In this case, we have

$$f*p = A \int d(z)\ p(ct-z)\ dz$$

$$= A \int d(z)\ \delta(ct-z)\ dz$$

$$= A\ d(ct) \quad . \tag{18}$$

Equation (18) states that the backscattered power is a faithful reproduction of the perturbation response (scaled by the amplitude of the probe pulse) when the perturbation is much larger than the width of the probe pulse.

In the second case, the width of the probe pulse is much greater than the perturbation, and the convolution, d*p, becomes

$$d*p = A\ p(ct) \quad . \tag{19}$$

Equation (19) states that the backscattered power is a faithful reproduction of the probe pulse. Hence, a narrow probe pulse yields the impulse response of the perturbation. On the other hand, a point defect can be identified by its resemblance to the probe pulse.

In the last case, where the perturbation is approximately the same width as the probe pulse, details of their shapes become important. In general, the response will not be a faithful reproduction of either the probe pulse or the perturbation, but will be wider than either.

This analysis indicates the tremendous potential of this technique for studying defects in waveguides. Point defects can be located with the OTDR and then examined to determine the source of the defect. Extended defects affect bound mode power in different ways; therefore, examining the OTDR signature provides clues about the origin of the defect.

SECTION 3

THE OTDR EXPERIMENTAL SETUP

Figure 4 shows the block diagram of an automated OTDR used in this program. One of the main features of this setup is the use of a polarization-isolation directional coupler based on a Glan-prism polarizer. This coupler is used in the OTDR since it reduces mount reflection, permits launch mode control, and is a non-destructive power launching method. Light from an injection laser is coupled into a fiber pigtail. (The pigtail facilitates source changes and provides a more nearly circularly symmetric launched spot.) The light output from the pigtail is collimated by the microscope objective, L_1. The collimated beam should be just large enough to completely fill the aperture of the lens, L_2. The Glan-prism polarizer transmits one polarization and dumps the power in the other polarization. For discussion purposes, we assume that the horizontal polarization is transmitted and the vertical is lost. A second microscope objective, L_2, focuses light onto the waveguide under test. (Maximum coupling efficiency is achieved if this lens has a numerical aperture identical to that of the waveguide.) The Fresnel reflection from the cleaved input endface of the waveguide under test remains horizontally polarized. As a result, this reflected light is not directed toward the detector; instead it passes through the prism polarizer and is lost. The backscattered power is collimated by lens L_2. Vertically polarized light is directed toward the detector by the polarizer. (Horizontally polarized light is transmitted through the prism polarize and lost.) A final lens, L_3, focuses the light onto the detector. A pinhole placed just in front of the detector helps reject stray light reflected from the mount. The directional coupler is simple to construct and can provide uniform excitation of all bound modes.

Individual bound mode groups can be launched in a step-index waveguide using a combination of apertures and stops in the spatial filter block following lens L_1. Apertures alter the size of the beam impinging on lens L_2. This causes the launch numerical aperture, NA_L, to vary according to

$$NA_L = b/f \quad , \tag{20}$$

11567-8

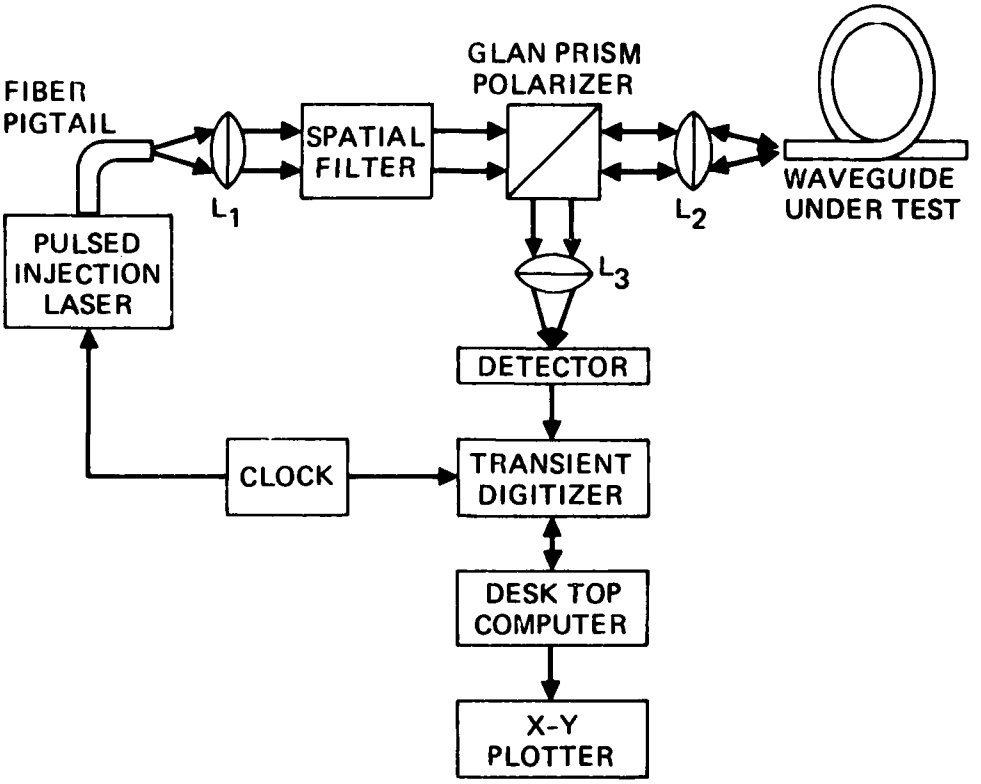

Figure 4.
Block diagram of an automated OTDR employing a Glan prism polarizer as the optical directional coupler. Only the horizontal component of the unpolarized, fiber pigtail output is launched into the waveguide under test. Only the vertical component of the unpolarized backscattered signal is sent to the detector. Consequently, the minimum total insertion loss of this coupler is 6 dB.

where 2b is the diameter of the beam entering L_2, and f is the focal length of lens L_2. The mode groups that are excited can be determined from

$$\frac{m}{M} = \frac{1}{\sqrt{2\Delta}} \quad \frac{b}{f} \quad , \tag{21}$$

where m is the principal mode group number, and M^2 is the number of bound modes in the waveguide.[5]

Although polarization rotated by 90° from the input polarization is detected, this usually presents no measurement problem. In standard multimode glass waveguides, light is depolarized within a few meters. This distance is small compared with the probe pulse width of the OTDR; consequently, the measurements are unaffected by a polarization-sensitive directional coupler. Complications occur if polarization-preserving waveguides are to be measured. (Polarization-preserving waveguides include single-mode and elliptical-core multimode waveguides.) Some method must be used to scramble the polarization if all modes are to be equally and independently excited in these waveguides.

Operation of the OTDR is straightforward. System synchronization is provided by the master clock. Timing pulses from the clock provide triggering information for both the transient digitizer and the pulse circuitry of the laser. The detected signal is amplified and fed into the transient digitizer. A complete OTDR characterization of the waveguide is recorded by the transient digitizer for each laser pulse. Digitizer resolution is 512 time cells by 512 vertical deflection cells. A predetermined number of individual characterizations are performed and averaged to increase the signal-to-noise ratio. The resulting waveform is sent to a desktop computer for processing and then to the X Y plotter for hard copy output.

The computer program which oversees data acquisition performs three functions. It determines waveguide length, supervises data acquisition, and analyzes data for hard copy preparation. Waveguide length is determined by measuring the elapsed time between the near- and far-end Fresnel reflections and multiplying by the group velocity. Data reduction consists of two parts: calculating the average optical power backscattered from each point along the waveguide, and determining the local attenuation. The result is a pair of X Y plots. The first is a semilogarithmic plot of backscattered optical power

versus position along the waveguide (referred to as the power plot). The second is a plot of local slope of the power plot (referred to as the loss plot). The loss plot is obtained from the raw data by performing a least-squares fit to an exponential over a time interval equivalent to the probe pulse width. The least-squares fit is performed for all the data points in the data array.

If the waveguide under test contains substantial attenuation variations, the computer program characterizes the waveguide from each end and then separates geometric variation from actual power decay. Local waveguide attenuation is determined from a least squares fit to the data of the actual power decay curve.

Figure 5 is a characterization of a waveguide obtained with this second program. The top of the figure shows that the waveguide exhibits very little geometric variation over length. Geometric variation is found from

$$I(z) = 10 \log \frac{f(z)}{f(L/2)} \quad . \tag{22}$$

Three separate curves are shown in the center of Figure 5. The solid curves are the characterizations from end 1 and end 2. The dashed line is the actual power decay curve. Notice that a small point insertion loss (0.17 dB) is present 400 m down the waveguide. The point insertion loss is even more pronounced in the local attenuation plot at the bottom of the figure. The origin of this point insertion loss is a single microbend. The other variations in the local attenuation are diameter variations.

Key performance specifications of this instrument are listed in Table 1. The directional coupler provides a mount scatter rejection of at least 20 dB at 0.9 μm. The directional coupler exhibits a total insertion loss of just under 10 dB which includes coupling losses into the fiber pigtail as well as losses due to the polarization properties of the prism polarizer. Typically, 100 mW of source power is coupled into the waveguide under test. The launch beam has a maximum 0.2 NA and a spot size of 50 μm. Typical pulse width is 130 nsec, which translates into a pulse 26 m long inside the waveguide.

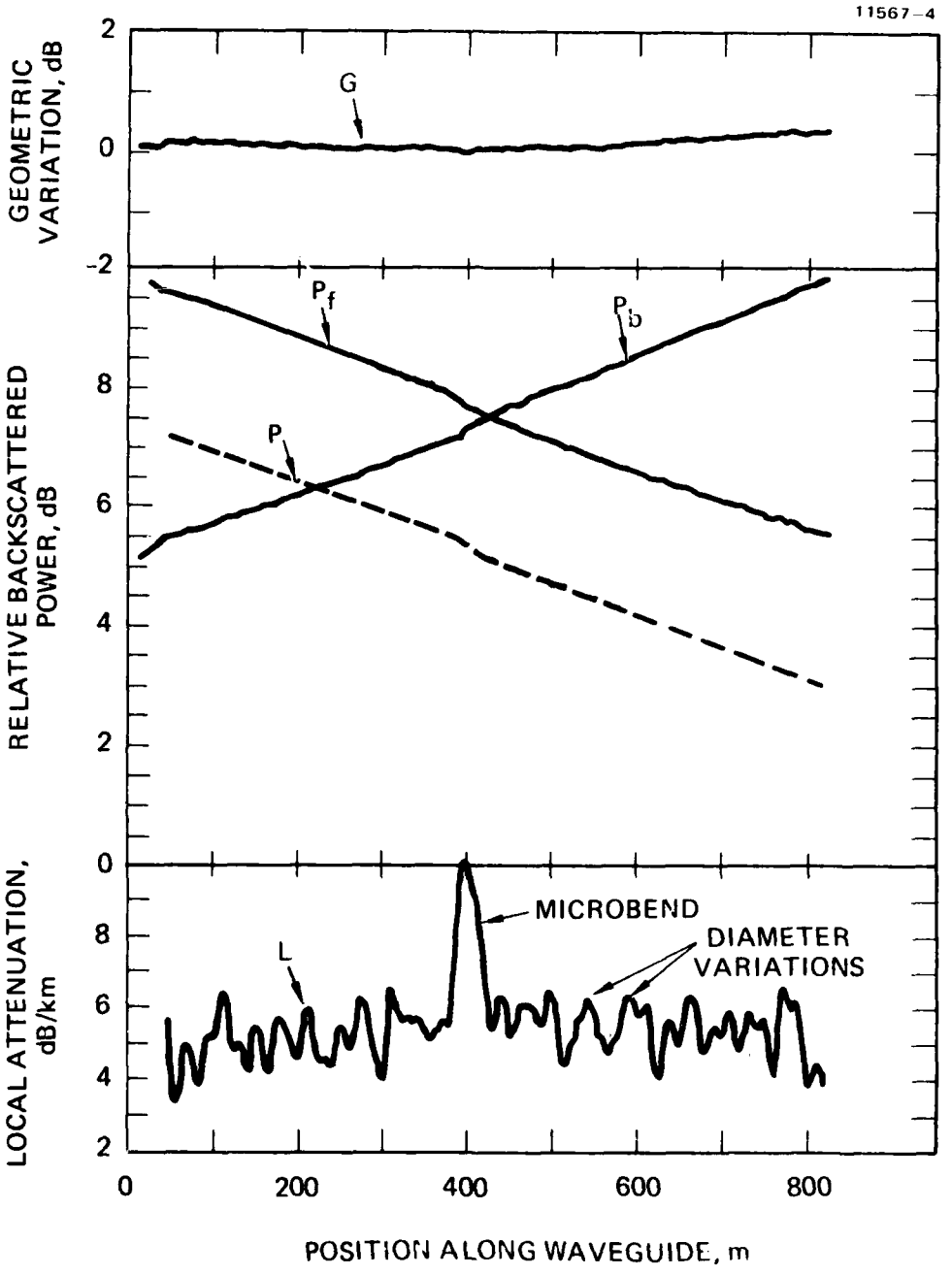

Figure 5.
Characterization of a waveguide with an automated OTDR. The waveguide was characterized from both ends, yielding curves P_f and P_b. This data was then analyzed numerically to separate the geometric variation, G, from the actual power decay, P.

Table 1. Key Performance Specifications of the Automated OTDR

Parameter	Typical Performance
Peak power coupled into waveguide at 0.9 μm	100 mW
Launch NA	0.2
Launch beam spot size	50 μm
Total insertion loss of directional coupler	<10 dB
Pulse width	130 nsec
Spatial resolution	26 m
Accuracy of length measurements	±2.5%
Dynamic range	50 dB, i.e., instrument can see through a waveguide exhibiting 25 dB attenuation
Fresnel reflection isolation of directional coupler	Exceeds 20 dB
Precision	±0.023 dB/km on waveguide exhibiting 7.64 dB/km attenuation
Accuracy	Within 4%

Length measurements are accurate to about 2.5%, limited by the resolution of the transient digitizer and the accuracy with which the waveguide group velocity is known.

A precision test consisting of 25 successive measurements of a single waveguide was performed using this apparatus. The waveguide is a 1-km-long, graded-index waveguide with 125 μm o.d., 62.5 μm core diameter, and 0.18 NA. For the precision test the probe beam spot size was 50 μm with a launch NA of 0.20. The mean attenuation was 7.64 dB/km at 0.9 μm with a standard deviation

of ±0.023 dB/km. This represents the highest precision yet reported for an OTDR. OTDR accuracy was determined by comparing OTDR measurements with measurements made on the same waveguide using the conventional cut-back technique. A total of 16 cut-back measurements on the waveguide yielded a mean attenuation of 7.81 dB/km with a standard deviation of 0.61 dB/km. (This measurement was also made with a 0.20 launch, NA, 50-μm-diameter spot size.) The agreement between measurements is within 0.17 dB/km (<4%).

SECTION 4

CONSIDERATIONS OF OTDR SENSITIVITY AND REPEATABILITY

As we pointed out earlier, one of the disadvantages of the backscattering technique is that the exact nature of the backscattering is unknown. For example, to obtain accurate attenuation data, it is necessary that the backscattered power be strictly proportional to the power present in the waveguide. If the backscattered power is a constant fraction of the power in the waveguide and the geometry of the waveguide does not change, then we have the simple case that the OTDR signal is directly proportional to the power in the waveguide (see Equation (10)). It was first assumed,[6] and later experimentally proven,[7] that the backscattered power has a λ^{-4} dependence and hence is Rayleigh scattering. Rayleigh scattering depends only on the material composition and fabrication technique and has a nearly isotropic angular distribution[8] over the NA within the waveguide. Therefore, in Rayleigh-scattering-limited waveguides, the backscattered power is strictly proportional to the power present in the waveguide. The lowest-loss waveguides manufactured today are Rayleigh-scattering-limited waveguides. Hence, the OTDR is expected to perform well on these waveguides.

An additional extremely important question is the distribution of the backscattered power among the bound modes of the waveguide.

Knowledge of the backscattered distribution is important because it has a direct impact upon OTDR perturbation sensitivity. We seek to locate and characterize perturbations using the backscattering method. Since each mode propagates with a characteristic attenuation (which is modified by the presence of a perturbation), complete characterization of the perturbation requires a knowledge of both the launch and backscattered modal distributions. As an example, consider a perturbed simple two-mode waveguide where mode 1 propagates with low attenuation and mode 2 with high attenuation. An OTDR characterization of this waveguide could result in four different permutations of the measured attenuation, depending upon modal excitation.

Our analysis provides an equation which can be used to determine modal excitation of backscattered light in α-profile waveguides. We assume no mode mixing and no differential modal attenuation. Under these conditions a WKB analysis[9] indicates that the radial variation of power is

$$p(r) = \frac{n^2(r) - n_2^2}{n_o^2 - n_2^2} \quad , \tag{23}$$

if all modes are excited equally at launch. The quantities in Equation (23) are

$$n^2(r) = \begin{cases} n_o^2 \left|1 - 2\Delta \left(\frac{r}{a}\right)^\alpha\right| & r < a \\ n_2^2 & r > a \end{cases} \quad , \tag{24}$$

$$\Delta = (n_o^2 - n_2^2)/2n_o^2 \quad . \tag{25}$$

The local numerical aperture, A(r), is

$$A(r) = n(r) \sin\theta_c(r) = [n^2(r) - n_2^2]^{1/2} \quad , \tag{26}$$

where

n_o = on-axis refractive index

n_2 = clad refractive index

a = core radius

α = a constant .

Since we have assumed no mode mixing and no differential mode attenuation, the power at any point along the waveguide is

$$p(r,z) = P_o e^{-\gamma z} \left(\frac{n^2(r) - n_2^2}{n_o^2 - n_2^2} \right) , \tag{27}$$

where P_o is the total power launched into the waveguide, and ν is the attenuation coefficient.

The fraction of light which is scattered in an annulus of radius r which is trapped in backward traveling rays is

$$F = \frac{1}{4\pi} \int_0^{2\pi} \int_0^{A(r)} \sin\theta d\theta d\psi \approx \left(\frac{1}{4} A^2(r) \right) , \tag{28}$$

where we assume the light is scattered isotropically. Consequently, the radial distribution of the backscattered power is

$$P_{bs}(r,z) = p_o e^{-\gamma z} \left(\frac{n^2(r) - n_2^2}{n_o^2 - n_2^2} \right) S \ \frac{1}{4} A^2(r)$$

$$= \frac{P_o S}{4} e^{-\gamma z} (n_o^2 - n_2^2) \left[1 - \left(\frac{r}{a} \right)^\alpha \right]^2 , \tag{29}$$

where S is the fraction of the pulse which is scattered at z.

The mode group m, excited by a ray which enters the waveguide at radius r, propagating at an angle θ with respect to the optic axis, can be found from[5]

$$\frac{m}{M} = \left[\left(\frac{r}{a} \right)^\alpha + \frac{\theta^2}{2\Delta} \right]^{(\alpha+2)/2\alpha} , \tag{30}$$

where M^2 is the number of modes in the α-profile waveguide. Inside the waveguide a bound ray will result if the ray forms an angle so that

$$0 < \theta < \sqrt{\frac{n^2(r) - n_2^2}{n(r)}} \quad . \tag{31}$$

Consequently, the mode groups which are excited by light scattered in an annulus of radius r are

$$\left(\frac{r}{a}\right)^{(\alpha+2/2)} < \frac{m}{M} < \left[\left(\frac{r}{a}\right)^{\alpha} + \frac{1}{2\Delta} \frac{n^2(r) - n_2^2}{n^2(r)}\right]^{(\alpha+2)/2\alpha} ,$$

which can be rewritten as

$$\left(\frac{r}{a}\right)^{(\alpha+2/2)} < \frac{m}{M} < \left[\frac{1 - 2\Delta \left(\frac{r}{a}\right)^{2\alpha}}{1 - 2\Delta \left(\frac{r}{a}\right)^{\alpha}}\right]^{(\alpha+2)/2\alpha} \approx 1 \quad . \tag{32}$$

Equation (31) provides us with knowledge of which mode groups are excited but does not determine how much power backscattered at radius r is coupled into each bound mode. To determine the power coupled into each bound mode we assume that each mode receives equal power and count the number of modes.

Each mode group, m, is m-fold degenerate. The lowest order mode group which is excited by light scattered from an annulus of radius r is D-fold degenerate, where

$$D = M \left(\frac{r}{a}\right)^{(\alpha+2)/2} .$$

The next higher order group is D + 1 fold degenerate; the highest order mode group is M-fold degenerate.

Therefore, the total number of excited modes is

$$N = 2\,[D + (D + 1) + \ldots + M] = M(M + 1) - D(D - 1) \quad , \tag{34}$$

where the factor of 2 accounts for the two possible polarizations. Finally, the power back-scattered from radius r into any allowed mode is

$$P_{mode}(r,z) = \frac{1}{2}\,\frac{P_o S n_o^2 \Delta\;\; 1 - (r/a)^{\alpha}\; 2 e^{-\gamma z}}{M(M + 1) - D(D - 1)} \quad . \tag{35}$$

Figure 6 shows the relative back-scattered power in various α-profile waveguides as a function of mode group number. Figure 7 shows the fractional change in mode group excitation assuming all modes are equally excited.

Source Considerations

Once the data acquisition system was verified we began looking into the question of the optimum source for this application. The backscattering which occurs in the fiber is described by a spatial function, b(z). (We assume the fiber is infinitely long for simplicity.) If a small intrusion perturbation, f(z), occurs along the fiber, the total backscattered signal is written b(z) + f(z). The OTDR probe pulse is a function of time, t, and position, p(ct - z). The temporal dependence of the backscattered signal, B(t), is

$$B(t) = \int (b(z) + f(z))\; p(ct - z)\; dz = \int (b(z)\; p(ct - z)\; dz + \int f(z)\; p(ct - z)\; dz \quad .$$

The first term in Equation (36) is the backscattering of the unperturbed fiber. The second term is the change in the backscattering caused by the intrusion perturbation. We wish to maximize the second term by tailoring the shape of the probe pulse.

Since the functions in Equation (36) are convolutions, the sensitivity is maximized by matched filtering. Ideally, we would tailor the probe pulse so that it is a matched filter for whatever perturbation is present.

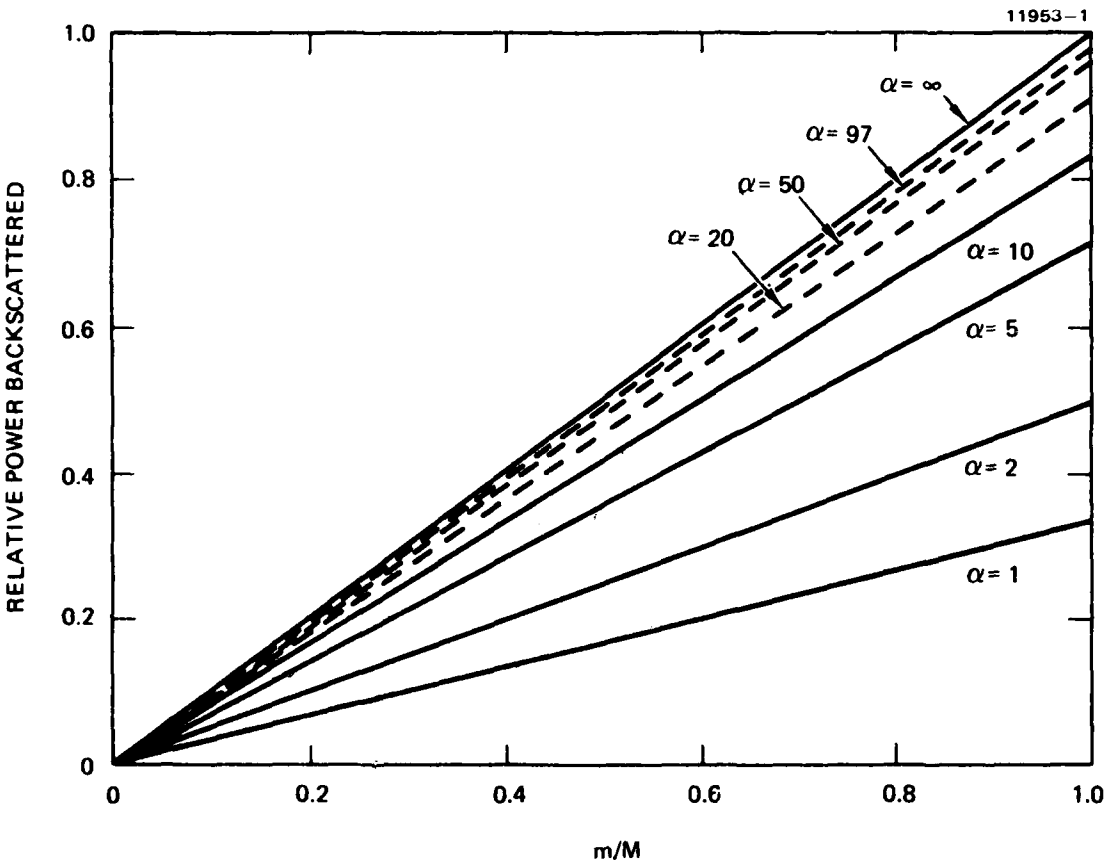

Figure 6.
Relative backscattered power in α-profile waveguides as a function of mode group, normalized to peak power and backscattered by a step-index waveguide.

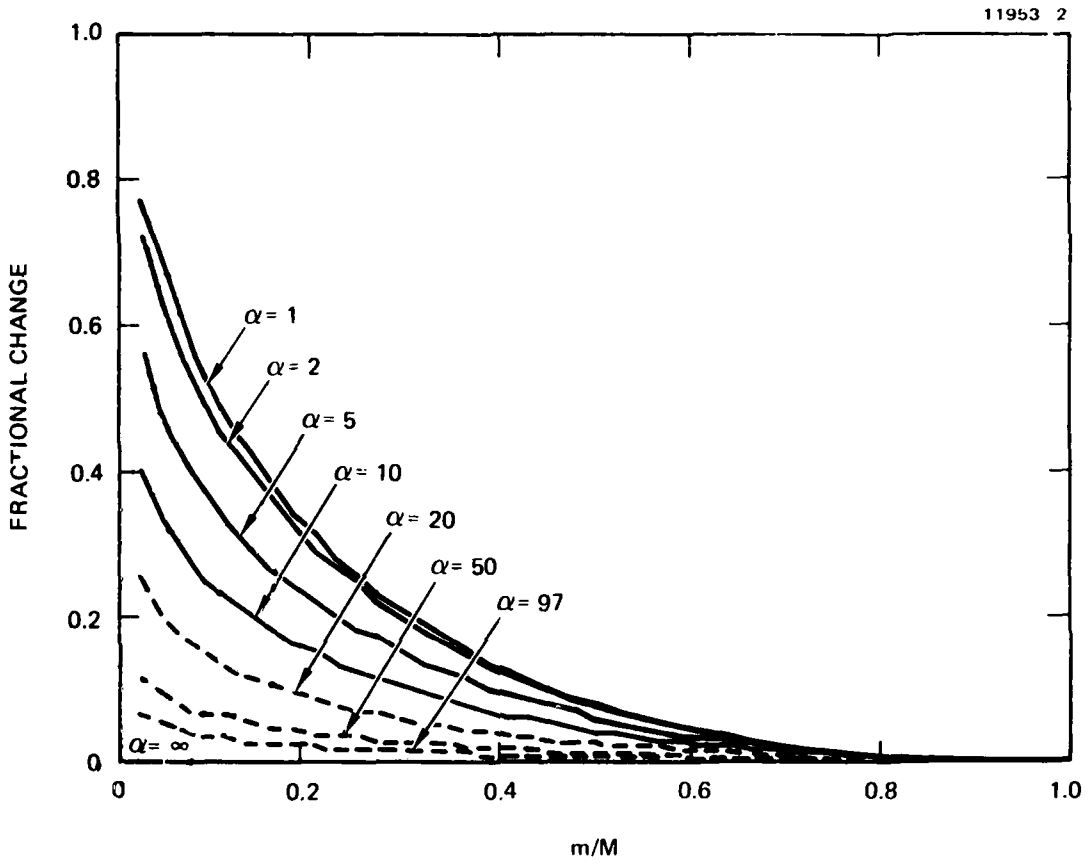

Figure 7.
Fractional change in modal excitation in α profile waveguides as a function of mode group.

Unfortunately, there are a large number of potential intrusions and we have no prior knowledge of which intrusion would be employed. The ability to generate a matched filter for each one would cause an inordinate level of complexity in the OTDR source electronics; therefore, a simpler approach must be found.

A better approach for a real system is to employ a wide probe pulse. Without resorting to detailed mathematical argument, several important reasons for using a wide pulse are given. If the probe pulse is narrower than the perturbation, the sensitivity is less than optimum. If the probe pulse is, roughly speaking, just as wide as the perturbation, the sensitivity is maximum; however, spatial resolution suffers. For near-term applications it is imperative to know that an intrusion is present rather than to know the fine structure in the backscattered return. We conclude that to maximize the sensitivity of the OTDR for a variety of perturbations a wide pulse is best.

There is, therefore, a tradeoff between the requirements of high spatial resolution and high OTDR sensitivity. To increase spatial resolution requires that the probe pulse width be decreased. (Eventually, in the quest for resolution the probe pulse width is reduced below the width of the perturbation and sensitivity suffers.) Assuming constant peak pulse power, a shrinking pulse width reduces the backscattered signal power proportionately.[10] The required detector bandwidth is inversely proportional to pulse width; hence, detector noise is inversely proportional to pulse width. Signal-to-noise ratio therefore drops as the square of the pulse width; hence, increasing resolution reduces sensitivity. Sensitivity may be increased by increased integration time. However, if the probe pulse width is reduced by a factor F, the required integration times will increase by F^2.

Laser diode sources alone are incapable of the peak powers required for submeter resolution. Increasing the spatial resolution of the OTDR requires either an increase in the peak optical power in each pulse, or electrically removing random noise. Since we are already pulsing our semiconductor laser sources at their maximum forward drive current, these sources require increased integration times to increase spatial resolution. An alternative is to go to other laser types such as an Nd:YAG laser.

Several benefits accrue from an Nd:YAG source. First, there is more than ample peak pulse power. In fact, most of the available power would be sacrificed to prevent stimulated effects and laser damage from occurring in the waveguide. In addition, the 1.06 and 1.3 μm wavelengths of this source are much closer to the lowest loss window in current fibers, thus permitting observation of substantially greater distances with the OTDR.

Several problems are associated with this solution. As the pulse width is reduced, the pulse repetition frequency, prf, goes down. A reduced prf requires more expensive detection and signal processing electronics, and requires longer data acquisition times. There is also a question of the reliability of the source. The only suitable commercially available laser which we have located is a Quantel laser. One of these lasers is already owned by HRL and is notorious for its alignment and reliability problems. This laser requires daily realignment, a serious drawback. The laser also exhibits a short mean-time to failure. These problems suggest that the best initial choice for a high spatial resolution OTDR is a semiconductor laser source and integration of the backscattered signal.

SECTION 5

OPTICAL FIBER PERTURBATION MEASUREMENTS

A. DETECTION OF SPLICES AND PERIODIC MICROBENDING

Experiments were performed to determine the OTDR signatures of splices and periodic microbending. Waveguides number 1 and 2 from a commercially available Corning 10 fiber cable were used in the experiment. Both waveguides exhibit essentially constant loss. Fiber 1 exhibits about 6.5 dB/km, while fiber 2 exhibits about 8.5 dB/km. Figure 8 presents the OTDR return obtained after fusing the two waveguides. The insertion loss of the splice was found to be 0.2 dB from the power plot. Notice that this splice was obtained by fusing end 2B to end 1B. The loss plot shows a monotonic decrease in the loss in fiber 1 following the splice. The monotonic decrease was seen in each of three fusion splices made with these waveguides and is attributed to the decay of leaky modes generated by the fusion splice. Finally, notice that fiber 2 now exhibits only 6 dB/km average attenuation, compared to 8.3 dB/km before splicing. This gross deviation in attenuation is not yet understood. The only known change that occurred in the experiment is that the launch end has been exchanged. We are now launching into end 2A, whereas the initial characterization was performed while launching into end 2B. A variation as large as 2.3 dB/km attenuation when launch ends are exchanged has not been observed previously.

A second set of experiments was performed to attempt to isolate a signature for periodic microbending structure. For this experiment, a microbending loss modulator was employed. The modulator uses a series of rods to bend the waveguide. The rods are spaced 3.5 mm apart, as shown in Figure 9. The waveguide follows a serpentine path between the rods exhibiting a bending period of 7 mm. Coupled mode theory predicts that this period is adequate to cause all lower order modes to couple, but insufficient to cause coupling among the highest order modes. Mass is applied to the upper plate in 50 gm increments, yielding the following peak-to-peak amplitude distortions in the fiber axis.

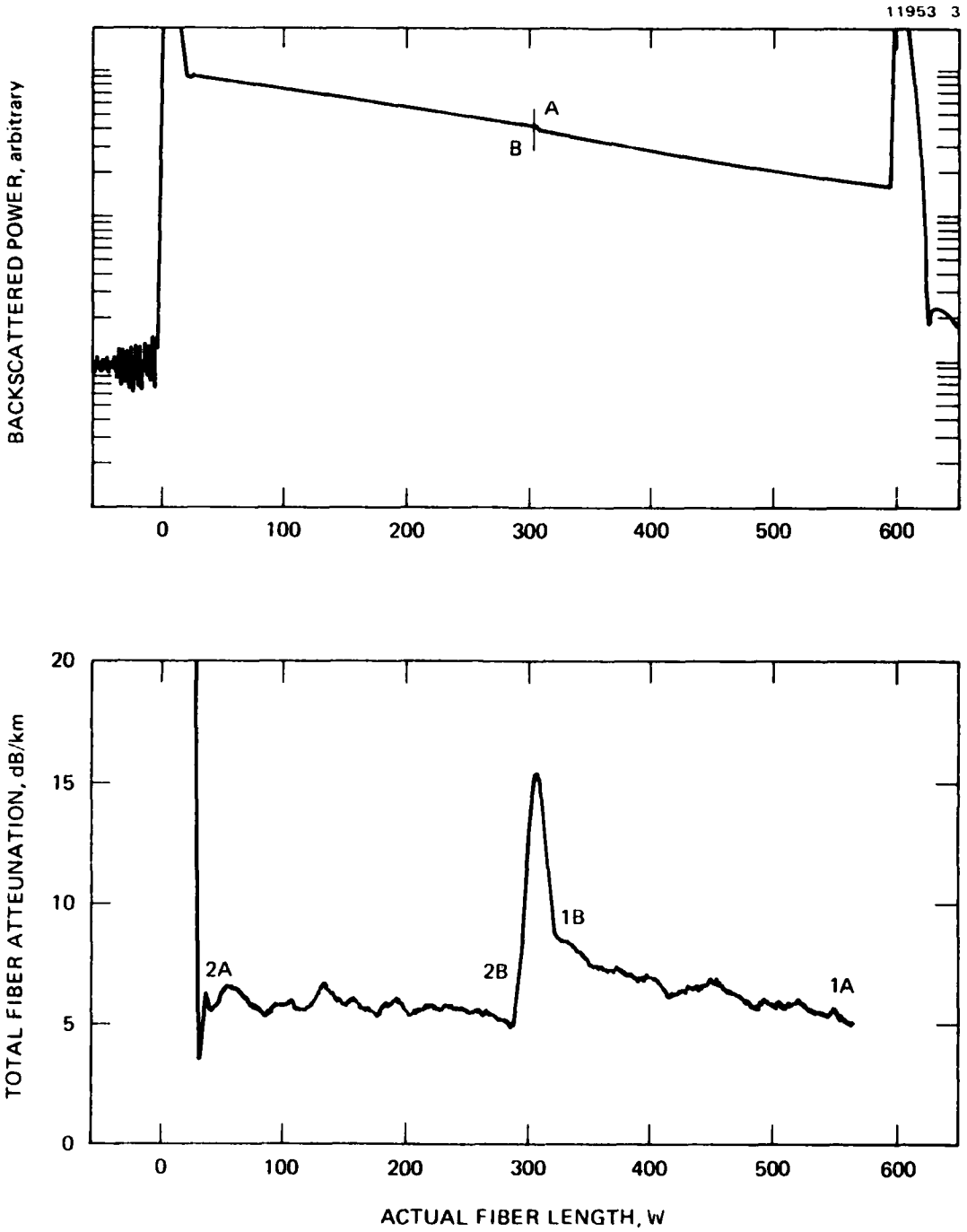

Figure 8. OTDR Characterization of a fuse-spliced fiber.

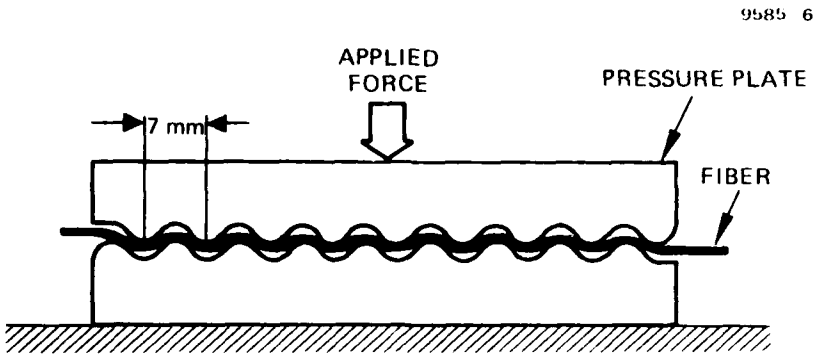

Figure 9. A microbending transducer.

Total Mass Applied, gm	Peak-to-Peak Distortion, μm
35	75
85	180
135	285
185	390
235	495

Figure 10 is a typical backscattered signal which resulted when the loss modulator was placed immediately after the splice. Notice the exponential drop in attenuation following the splice and modulator. This drop is due to the attenuation of leaky modes excited at the splice. It was observed that the loss in fiber 1, immediately adjacent to the splice, monotonically increases with distortion amplitude; however, at the time the pulse arrives at the far end of the waveguide, the loss is back to its initial (unperturbed) 6.5 dB/km loss.

The modulator was also placed immediately before the splice and the experiment repeated. The results were nearly identical. Both the splice and the loss modulator introduce a point insertion loss and cause mode conversion

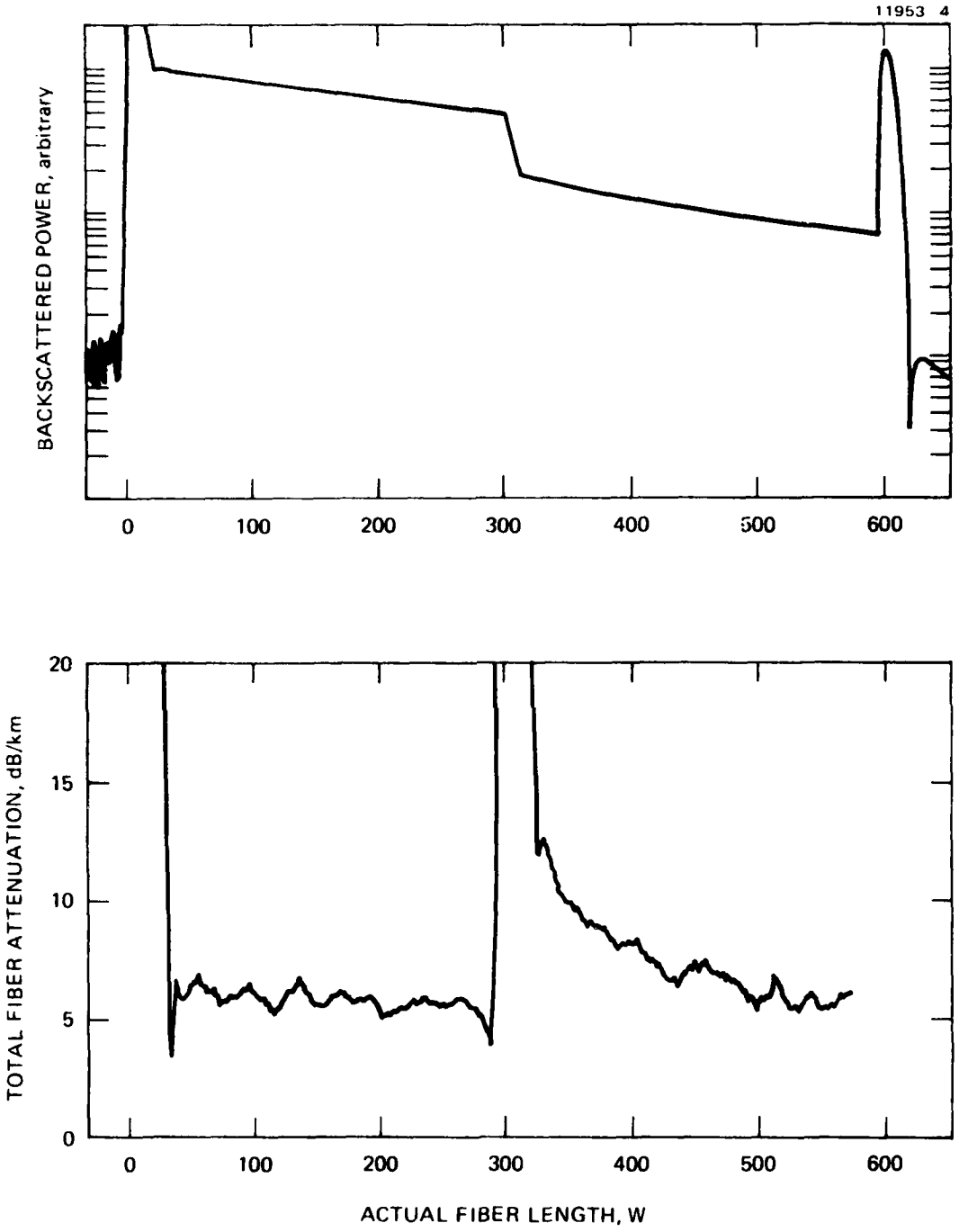

Figure 10. 0.9 μm OTDR characterization of a fuse-spliced fiber with a loss modulator placed immeidated after the splice.

to leaky modes. If the two perturbations occur in series, the order has little effect.

A final experiment was performed using only the bending loss modulator and fiber 2. The bending loss modulator was placed immediately after the launch. Figure 11 shows the result of this experiment. Note that the change in the OTDR characteristic is only about half of the change which was observed in the original experiments during which a splice was present. This difference is due to mode conversion in the splice.

Extremely small displacements of a microbend transducer have been reliably located and measured with the OTDR. The transducer consists of two mating plates with milled grooves (1.5 mm spacing) into which stainless steel rods (500 μm diameter) are cemented. The transducer thus provides a minimum mechanical distortion period of 1.5 mm which can be increased by removing pins or by altering the angle between the fiber axis and the pin axes. The fiber is subjected to a total of thirty-one bends in the transducer.

The results of experiments performed on this transducer are shown in Table 2. Displacements were measured using a linear voltage displacement transducer calibrated at 1.22 mV/μm. The small displacements measured during the experiments with the hydrophone transducer lead to questions of accuracy. it seems unlikely that the hydrophone transducers is mechanically perfect. It is particularly unlikely that the tops of the pins in the transducer all lie in a single plane. It is far more likely that if a plane were drawn through the mean pin height, some pins would protrude above that plane and some would be recessed. To insure that the tops of all the pins lie in the same plane requires some sort of polishing operation be performed on them.

A simple alternative approach is a single bend transducer employing only three pins. If a thin conductive coating is also applied to the waveguide, a conductivity measurement makes it possible to determine when this fiber is just in contact with all three pins. This is a convenient reference point corresponding to the point where the waveguide just begins to bend.

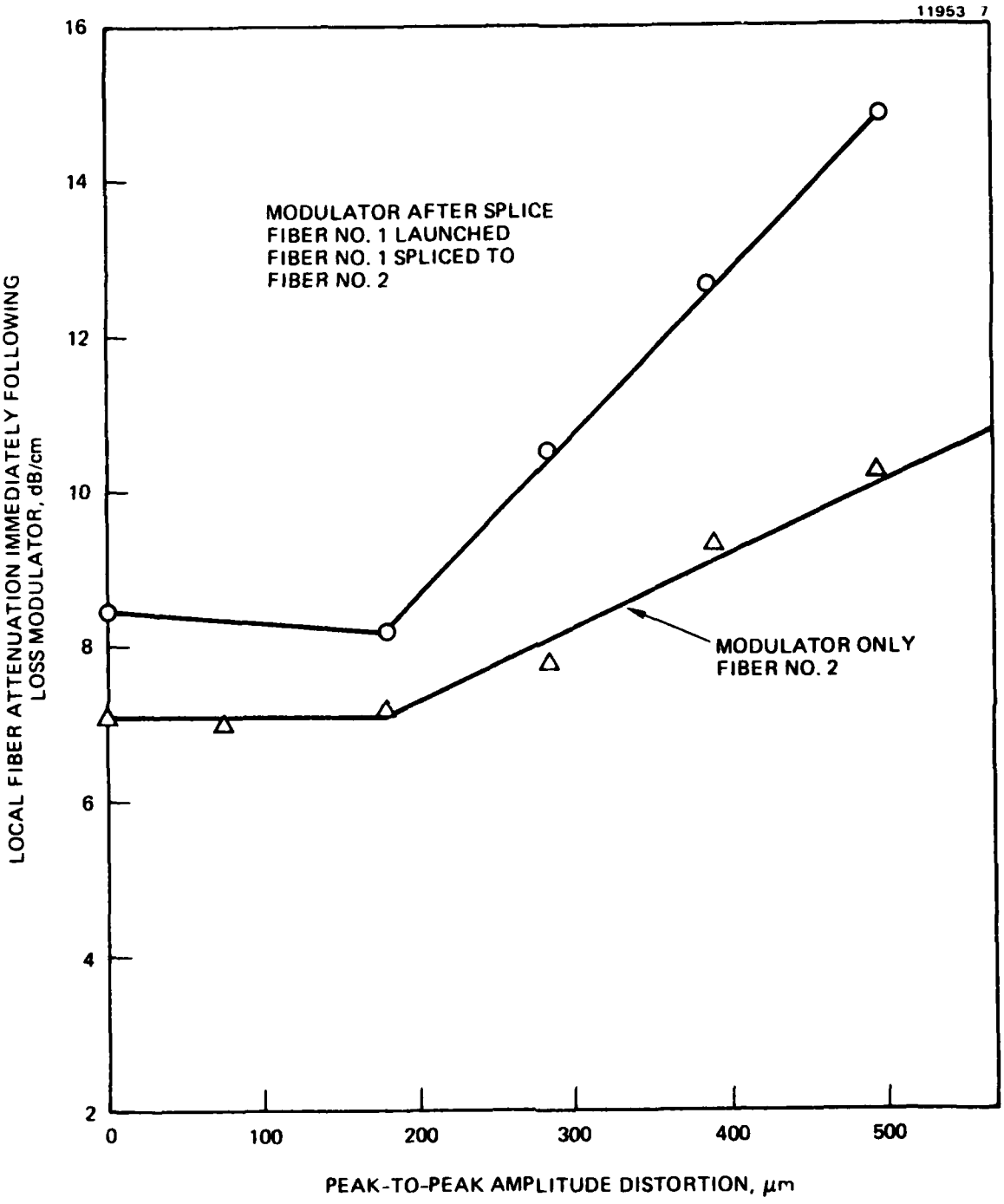

Figure 11. Local fiber attenuation immediately following the splice as a function of the peak-to-peak amplitude distortion of the fiber axis.

Table 2. Attenuation of the Microbend Transducer

Experimental Conditions	Spatial Period Λ, mm	Peak-to-Peak Distortion Amplitude, μm	Two-Pass Insertion Loss, dB
Dry, all modes excited equally	1.5	3	0.30
		6	0.62
		8	1.16
Dry, all modes excited equally	2.1	10	0.04
		13	0.04
		14	0.10
		20	0.31
Wet, index matching fluid n = 1.51, all modes excited equally	2.1	0	0.02
		5	0.21
		11	0.93

B. DETECTION OF A SINGLE LOOP IN A FIBER

Experiments designed to collect signatures of various perturbations have been carried out. One of the perturbations is a simple fiber loop.

There is a simple method for determining the presence of a loop using the OTDR. It is known that modes with a principal mode number, m, approximately equal to or greater than a critical value, m_c, defined by

$$\frac{m_c}{M} \approx \left(1 - \frac{a}{\Delta R}\right)^{1/2} , \tag{37}$$

are essentially and instantly lost in a simple bend. The variables in this equation are the core radius, a, the index difference between core and clad, Δ, the radius of the bend, R, and the total number of mode groups, M. In step-index waveguides there is a simple relat ' ship between the principal mode number and launch angle of a collimated beam. That relationship is

$$\frac{m}{M} = \frac{\sin\theta}{\sin\theta_{max}} , \tag{38}$$

where θ is the angle of the beam with respect to the optic axis, and θ_{max} is the critical angle for total internal reflection. Hence, we have a simple method of determining whether a fiber has a bend in it, and even for determining what the radius of the bend is. If the OTDR measures no excess loss at the location of the loop when $\theta = 0$, and large excess loss when $\theta = \theta_{max}$, a loop is present. (This conclusion, of course, assumes that little or no mode mixing occurs in the fiber.) If we measure the critical angle, θ_c, for which the OTDR begins to measure large excess loss, we can deduce the bend radius from the expression

$$\frac{m}{M} = \frac{a}{\Delta} \frac{1}{1 - \left(\frac{\sin \theta_c}{\sin \theta_{max}}\right)^2} \quad . \tag{39}$$

A standard Corning step-index waveguide was used for this experiment. The waveguide has an NA of 0.184, an outer diameter of 125 μm, and a core diameter of 85 μm. Most of the waveguide is on the standard 12-cm Corning shipping spool. Approximately 125 m have been wound onto an identical 12-cm spool (see Figure 12). A loop was formed between the two spools and it was placed in an index matching fluid. The initial loop diameter was 12.6 cm. measurements were made at 10 loop diameters between 2.1 and 12.6 cm. The results of the experiment are shown in Figure 13. For this experiment all mode groups were excited with approximately the same power.

We have also measured the excess attenuation induced by a loop using five different launch modal configurations. The configurations are summarized in Table 3. The results are plotted in Figure 14, along with a simple theoretical prediction determined from the formula:

$$\text{Loss} = 5 \log \left(1 - \frac{a}{\Delta R}\right) \quad , \tag{40}$$

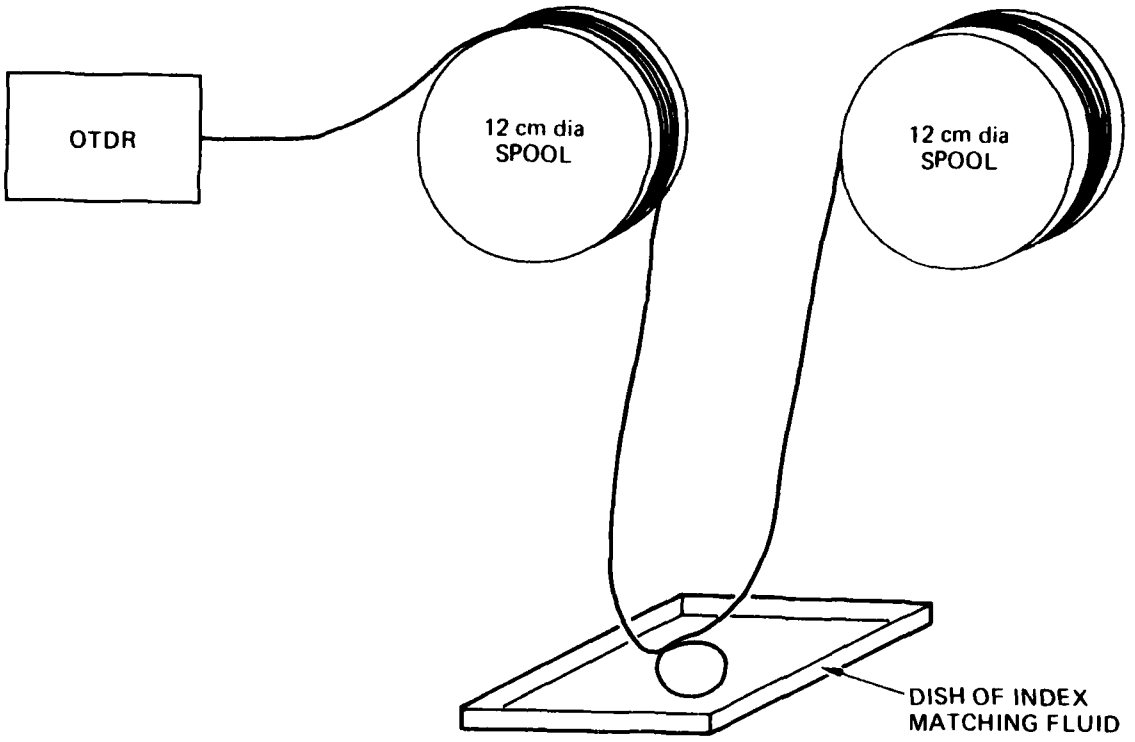

Figure 12. The experimental setup for detecting a single fiber loop. A single loop of fiber from the middle of a long fiber is immersed in index matching fluid.

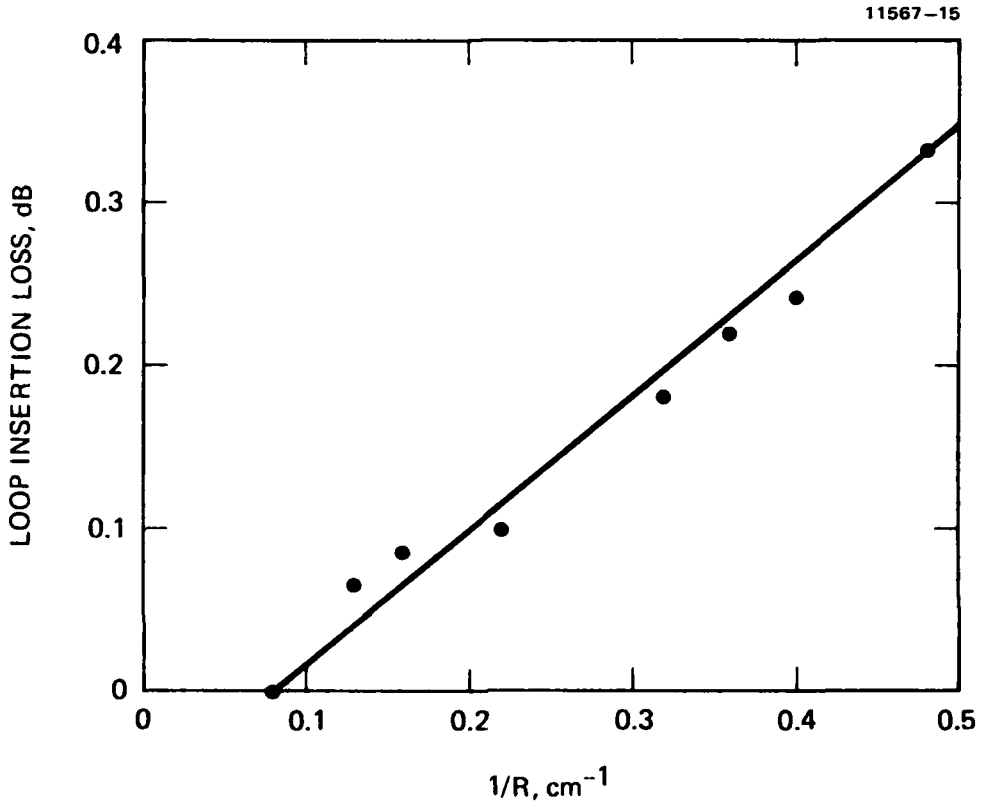

Figure 13. The observed attenuation of a single loop of waveguide when all modes are equally excited.

where R is the radius of the loop. The curve labeled "A" in Figure 14 presents data obtained from two different experiments. For the first experiment, the focused spot was placed at the center of the core. For the second experiment, the focused spot was placed at the core-clad boundary. Virtually identical results were obtained as expected.

The larger excess loss for lower order mode excitation as compared to the intermediate mode group is not understood. Note that the OTDR can only detect loops as large as 8 cm in diameter. Larger diameter loops might be located if the signal-to-noise ratio is improved.

C. MEASUREMENT OF THE INSERTION LOSS OF A SINGLE MICROBEND

A possible technique for taping an optical fiber is microbending. Microbends are microscopic bends at the optical axis which are short enough to cause mode conversion. If mode convertion is present, power which was bound to the core can be converted to even high order modes until it is finally lost to radiation. The power which is lost is then available for use by the intruder.

Under this contract we have measured the sensitivity of the OTDR to the presence of the microbends. Single microbends as small as 10 μm in amplitude and 1.5 mm in extent were observable. The OTDR response was found to be nearly quadratic in microbend amplitude.

The computerized OTDR, described in Section 3, was used to characterize the microbend.

Table 3. Details of the Launch Modal Configurations used in the Initial Loop Detection Experiments

Launch Configuration	Aperture Opening, mm	Stop Diameter, mm	Launch NA	Focused Spot Size, μm	Approximate Mode Groups, Launched
A	10.0	0	0.20	5.0	0 - 53
B	6.5	0	0.13	7.6	0 - 34
C	3.5	0	0.07	14.0	0 - 18
D	6.5	3.5	$0.07 < NA < 0.13$	—	18 - 34
E	10.0	6.5	$0.13 < NA < 0.20$	—	34 - 35

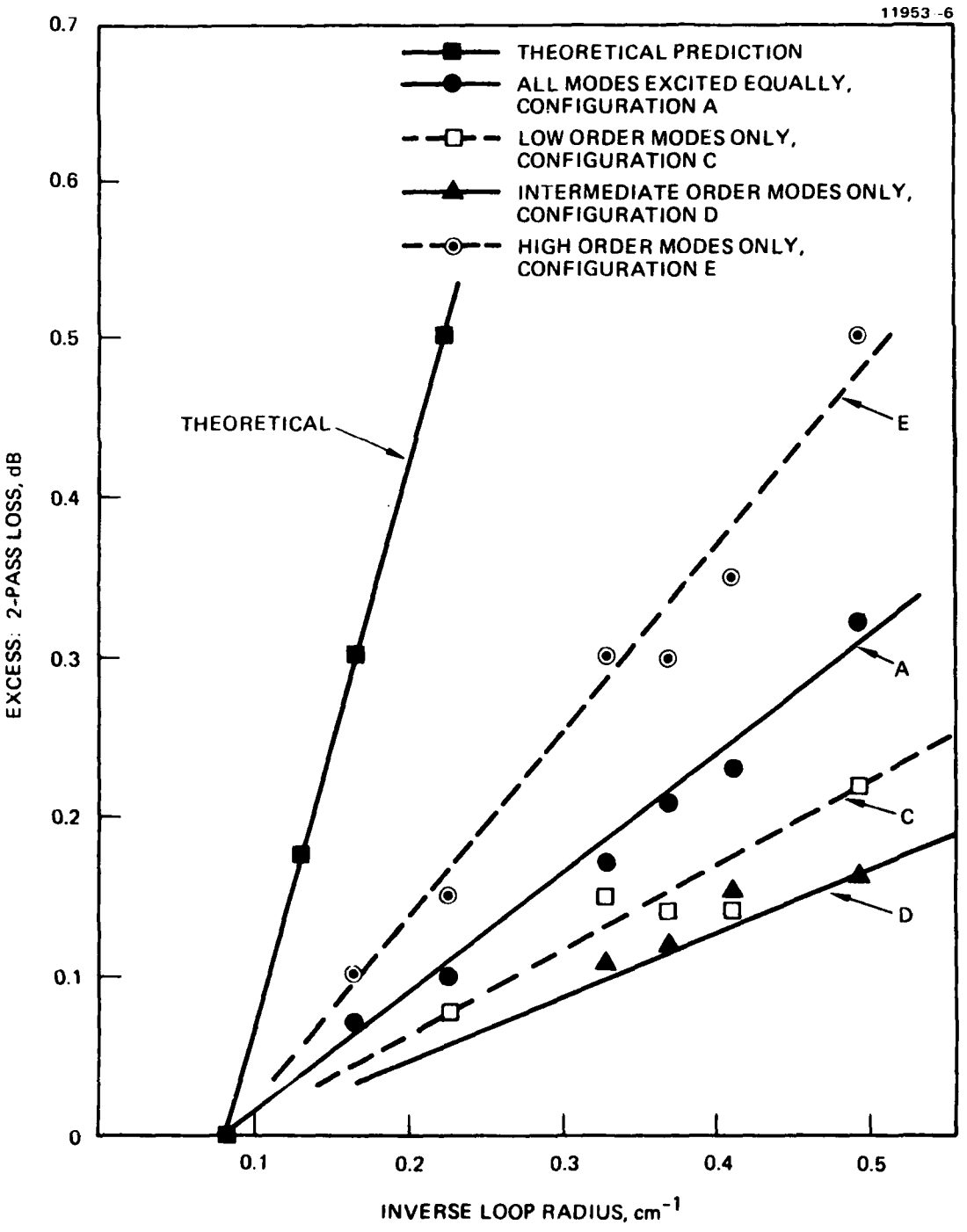

Figure 14. Excess loss as a function of inverse loop radius for a step-index fiber.

A 300-m-long high-quality step-index waveguide was used for this experiment. The core diameter is 84 μm, the outer diameter is 126 μm, the numerical aperture is 0.20, and the mode mixing length[10] is 670 m.

The microbending experimental setup is shown in Figure 15. Sixty meters of the fiber are wound on spool A and the remainig 270 m are wound on spool B. Between the spools is the microbend transducer, which is in turn mounted on a precision vertical translation stage (Klinger UH-80PP). This stage provides 1 ± 0.5 μm vertical steps on command from the controller. The transducer plates have many parallel grooves, spaced 1.5 mm apart, milled into the contacting surfaces. Two steel drill blanks, 0.53 mm in diameter, are cemented into the upper plate in adjacent slots. One drill blank is cemented into the bottom plate in a slot centered between the two upper rods. This arrangement provides a single microbend of 1.5 mm period when the waveguide axis is normal to the drill blank axis. (The period can be changed by rotating the transducer). An integrating sphere collects the OTDR probe-pulse power transmitted by the waveguide. A lockin amplifier (PARC 124) measures the

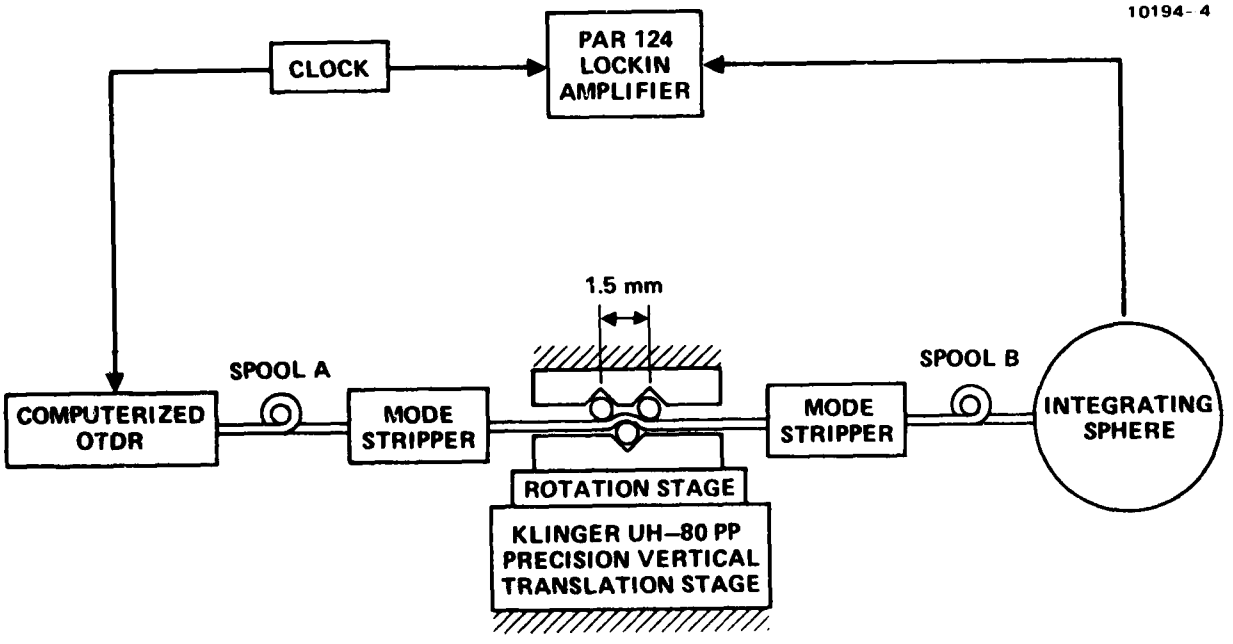

Figure 15. The microbending experimental setup.

power collected within the sphere. Simultaneous measurement of the transmitted power provides an insertion-loss measurement check on the accuracy of the OTDR data.

Preliminary experiments demonstrated that the OTDR is extremely sensitive to the presence of microbending perturbations. This forced the use of a positive method for determining when the pins just touch the waveguide The solution chosen was to immersion silver the waveguide. Approximately 1 μm of silver is deposited on the waveguide by this process. The overcoated waveguide is placed in the microbending fixture and electrical leads are attached to all three drill blanks. The bottom plate of the microbending fixture is stepped up in 1 μm steps to the point where electrical continuity is just obtained between all three pins. Microbend amplitude is measured with respect to this reference point.

Typical OTDR microbend characteristics are presented in Figure 16. The top half of the figure presents characterizations of the unperturbed waveguide and microbends of 10- and 25-μm amplitude. The bottom half of the figure presents the change in the local attenuation attributable to the presence of the microbend. These difference curves were obtained by subtracting the local slope of the unperturbed waveguide characterization from the local slope of the characterizations obtained when the three bending pins just touched the waveguide, when a 10-μm perturbation was present, and when a 25-μm perturbation was present. The insertion loss of the microbend was determined by integrating the area under the difference curves. Note that there is no reflection occurring at the microbend. Only loss is present.

The experimental results are shown in Figures 17 and 18. Figure 17 shows insertion loss as a function of microbend amplitude for two different rod spacings, 1.5 mm and 2.1 mm. The solid curves were obtained from the OTDR data, while the dotted curves are insertion loss measurements. The maximum difference between corresponding measured values is 0.074 dB. The hard primary coating was removed from a small length of the fiber. Adjacent segments of coated and uncoated waveguide were immersion silvered. Microbends were introduced into each segment and identical insertion losses were measured. The data fit well to a square law formulation, as shown in Table 4. (The single data point at 25-μm distortion amplitude, 2.1-mm period was deleted when calculating the best power law fit.)

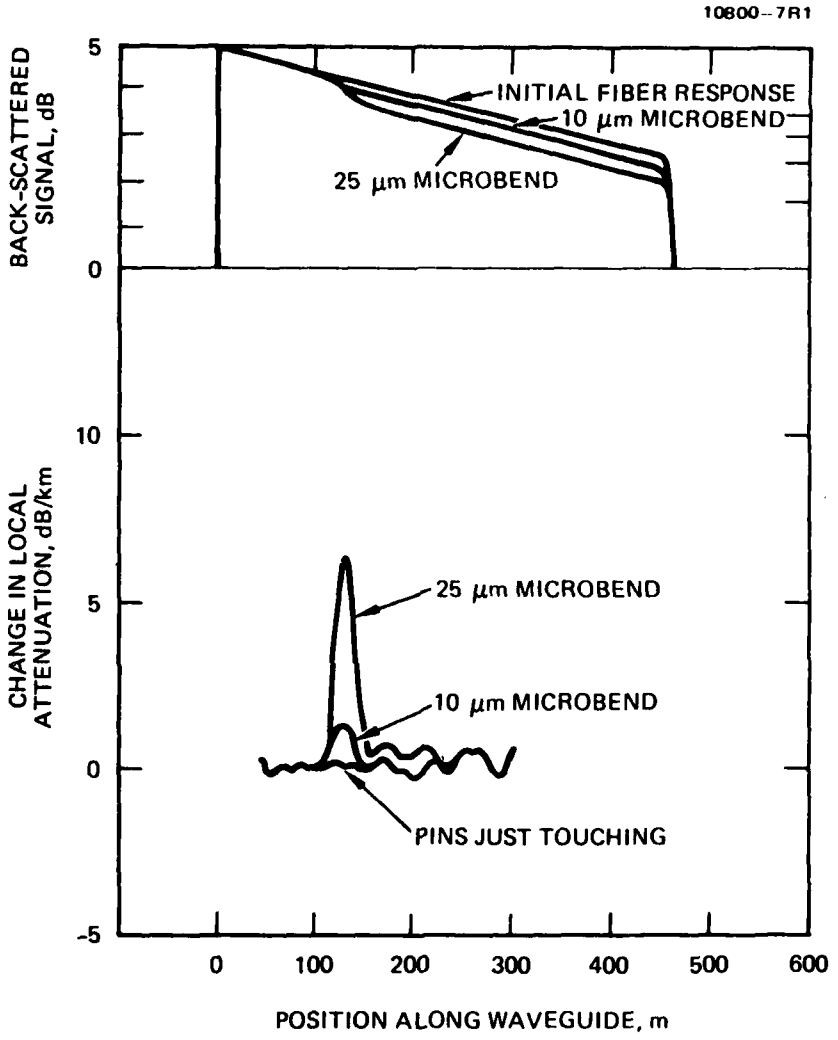

Figure 16. Typical OTDR microbend characteristics.

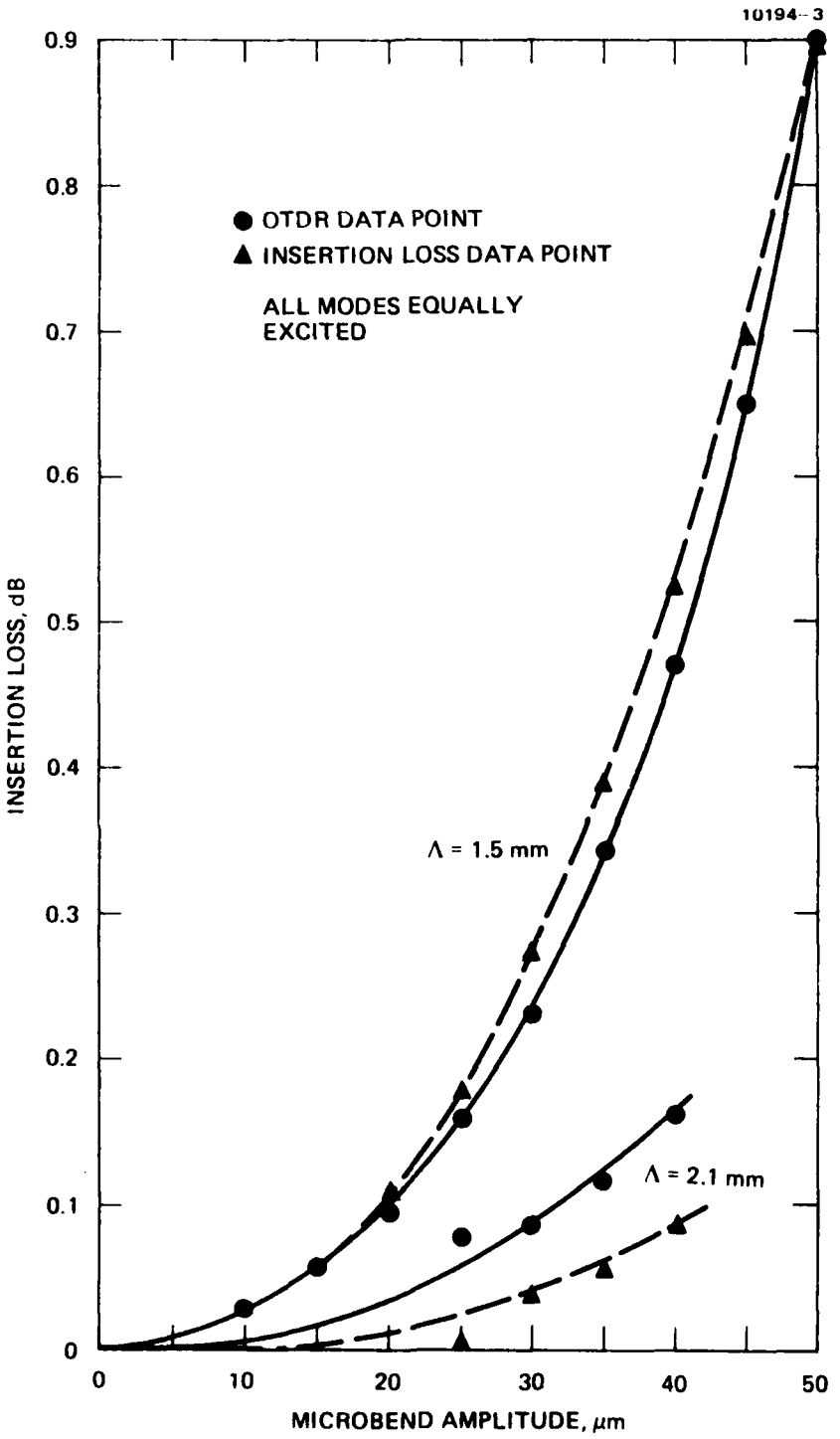

Figure 17. Microbend insertion loss dependence on the square of the microbend amplitude.

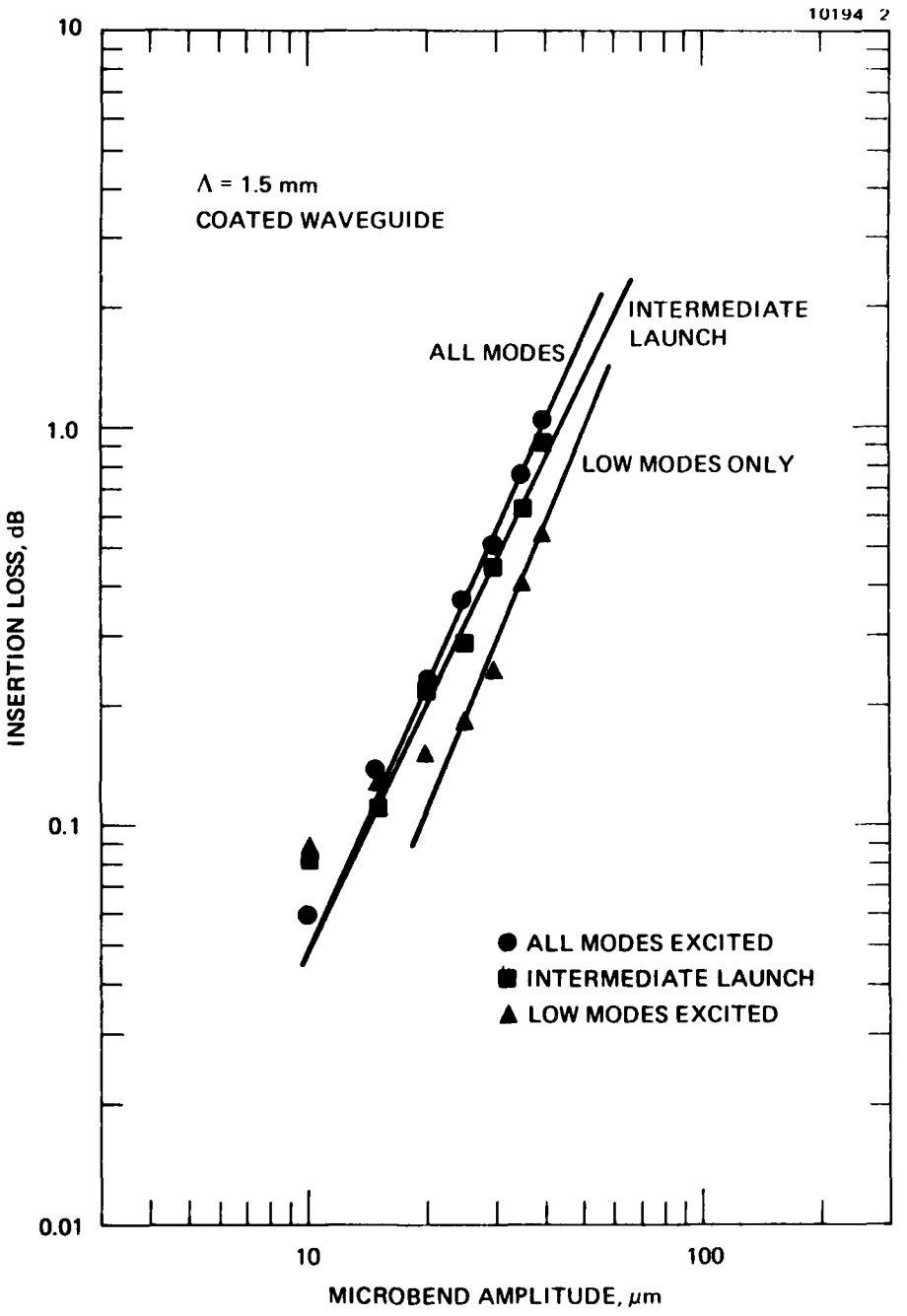

Figure 18. Microbend insertion loss as a weak function of launch mode configuration.

A dependence on the square of the distortion amplitude is expected. The average power coupling which occurs between modes of any principal mode group is proportional to the power spectrum of the fiber distortion.[11] The distortion applied to the fibers is a truncated sinusoid with amplitude A. Thus the bending power spectrum is proportional to the square of the distortion amplitude.

Only a slight dependence on launch mode configuration was observed (see Figure 18). This figure compares the measured results for the cases of low, low and intermediate, and all modes launched. The waveguide has a maximum mode group number of 48 at the measurement wavelength of 0.9 μm. The low mode launch excites mode groups 1 through 20.. The low and intermediate mode launch excites groups 1 through 38.

Relative insensitivity to mode group excitation is expected since this is a step-index waveguide. In step-index waveguides, the difference in propagation constant between adjacent modes depends upon the mode group number M according to[12]

$$\delta\beta = \frac{2\sqrt{\Delta}}{a}\left(\frac{m}{M}\right) , \tag{41}$$

where Δ is the relative index difference between core and clad, a is the core radius, and M^2 is the number of bound modes in the waveguide. Coupling will occur between mode groups i and j if their propagation constants are related to the mechanical period, Λ, of the perturbation through the expression

$$\beta_i - \beta_j = \frac{2\pi}{\Lambda} . \tag{42}$$

Perturbations with spectral components of longer or shorter period will not couple power efficiently. The largest intramode group jump occurs between the highest and second highest mode groups. No significant conversion of bound mode power to radiation modes can occur unless power is coupled across this gap. Nonsinusoidal mechanical perturbations short enough to couple these mode groups can be expected to contain sufficient low-frequency spectral components to couple all lower lying mode groups. Longer period perturbations impart insufficient momentum to the mode group to permit coupling across the largest "propagation constant gap."

Table 4. Experimental Results

	Induced Attenuation, dB			
	Λ = 1.5 mm		Λ = 2.1 mm	
Distortion Amplitude, μm	OTDR Data	Insertion Loss Data	OTDR Data	Insertion Loss Data
0	0	0	0	0
5	—	—	—	—
10	0.026	0.026	—	—
15	0.058	0.058	—	—
20	0.091	0.104	—	—
25	0.155	0.176	0.079	0.005
30	0.232	0.271	0.083	0.037
35	0.343	0.388	0.115	0.054
40	0.470	0.524	0.160	0.086
45	0.648	0.693	—	—
50	0.901	0.893	—	—
Best fit power law	2.2	2.2	2.3	2.9
Coefficient of correlation	0.99	1.00	1.00	0.99

D. MEASUREMENTS OF FIBER DIAMETER VARIATIONS

If all the high order modes of a multimode waveguide are populated with an equal amount of power, and if the diameter of the waveguide decreases, then some of these modes are cut off and the power they carry is lost. Virtually all waveguides have some diameter fluctuations. Power is available to an intruder if it can locate a diameter variation point and if power is lost at this point.

The OTDR can be used to identify points where such an intrusion might be attempted. Consider a narrow pulse of light propagating along a waveguide. The pulse suffers a position dependent attenuation described by the attenuation coefficient, $\gamma_f(z)$, composed of a scattering term, $\gamma_{fs}(z)$, and an absorption term, $\gamma_{fa}(z)$. The change in pulse power, $dP_f(z)$, is linearly proportional to the pulse power according to

$$dP_f(z) = -\gamma_f(z)\, P_f(z)\, dz \quad , \tag{43}$$

which can be rewritten as

$$P_f(z) = P_o \exp\left[- \int_o^z \gamma_f(x)\, dx \right] , \tag{44}$$

where P_o is the initial peak pulse power. The backscattered power, P_b, is some backscattering function, f(z), of the power at position z. The backscattering function depends upon waveguide geometric properties (NA and core diameter) as well as the scattering coefficient. Scattering sites encountered by the probe pulse are most commonly microscopic Rayleigh scattering sites. These sites scatter nearly isotropically, permitting a simple first order calculation by the waveguide acceptance, NA, at the scattering site by 4π. The backscattering function is simply the fraction multiplied by the scattering coefficient. For a step-index waveguide the backscattering function is[10]

$$f(z) \approx \frac{\gamma_{fs(z)}}{2} \, \frac{NA^2(z)}{n^2(z)} \quad . \tag{45}$$

The backscattered signal suffers position dependent attenuation, $\gamma_b(z)$, on the return trip. Collecting these results, we find that the power which is backscattered from the pulse at point z and is subsequently detected is

$$P(z) = CP_o f(z) \exp\left[-\int_o^z (\gamma_f(x) + \gamma_b(x))dx\right] \quad . \tag{46}$$

The quantity C is the coupling efficiency of the directional coupler. Now consider a waveguide containing core diameter fluctuation.

Since the number of bound modes, N, depends on the core radius, a, according to

$$N = \frac{(ka\ NA)^2}{2} \quad , \tag{47}$$

changes in radius cause corresponding changes in the number of bound modes. Mode coupling cannot occur if the period, Λ, is large. Higher order modes must become leaky, causing excess attenuation which can be lumped into the absorption coefficient. If the bound mode excitation is constant, independent of position and independent of direction of travel, then a sinusoidal variation in core radius of the form

$$a(z) = a_o\left[1 + B \sin(\ell z)\right] \tag{48}$$

modulates the attenuation coefficient according to

$$\gamma = \gamma_t + \gamma_a m(z) \sin(\ell z) \quad , \tag{49}$$

where ℓ is $2\pi/\Lambda$, and m(z) depends upon the properties of the waveguide. If the backscatter function and the modulation depth are constant, the power backscattered as a function of position is given by

$$P(z) = P_o f e^{-2\gamma z} \exp\left[-\frac{2\gamma_a m}{\ell}(1 - \cos(\ell z))\right] . \tag{50}$$

Figure 19 is the first reported observation of diameter variations made with the OTDR.[11] The figure shows a characterization of a step-index waveguide which was manufactured without the aid of a diameter stabilization system. The lack of stabilization resulted in peak diameter variations of ±32 μm around the mean waveguide diameter of 120 μm. The period of the variations is about 100 m. Note the one-to-one correspondence between peaks in backscattered signal and local minima in the waveguide diameter.

Much more subtle diameter variations can be seen in most commercially available waveguides. The signature of one such waveguide, a high-quality, graded-index waveguide manufactured by ITT, is shown in Figure 20. The signature shown here was obtained when all modes were equally excited by the probe pulse. There are many very small deviations from linearity in this characterization. To accentuate them, the local slope of the curve was measured and is also shown here. Notice that the local attenuation varies nearly sinusoidally with position.

It was not possible to remove the primary coating from this fiber in order to measure the actual outer diameter. (This particular waveguide was destined for an application requiring that its initial high strength be maintained. The fiber had passed a 200 kpsi proof test.) To verify that diameter fluctuations were responsible for this observed attenuation behavior we contacted the manufacturer and asked for their diameter chart. ITT graciously provided that chart. The measured fiber diameter is shown in Figure 21. Note that there are sinusoidal diameter variations; however, the amplitude is quite small, about 2.5 μm peak corresponding to an RMS variation <1.5% of the OD. Also shown is the local attenuation from Figure 20 and the superposition of the two curves. There is excellent correlation between them. From this data we estimate the sensitivity of the OTDR to sinusoidal diameter variations to be about 1.5 dB/km/μm change in core diameter. Note also the high spatial frequency diameter variations. These variations are also visible in the local waveguide attenuation data in spite of the fact that these variations are typically 10 m in width (which is much narrower than the OTDR probe pulse width of 25 m).

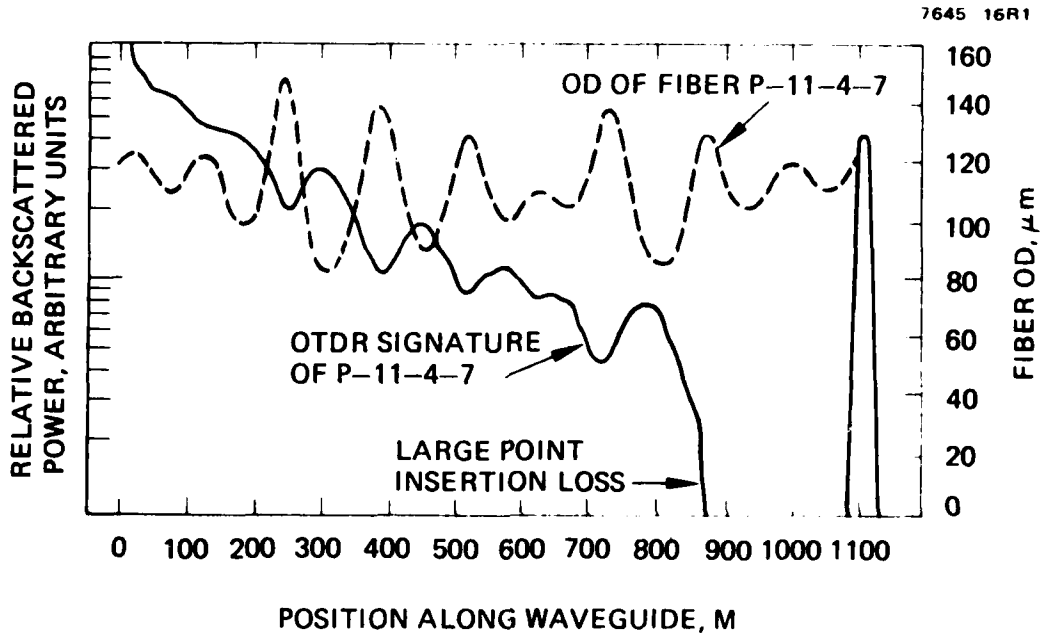

Figure 19. First reported observation of diameter fluctuations made with the OTDR.

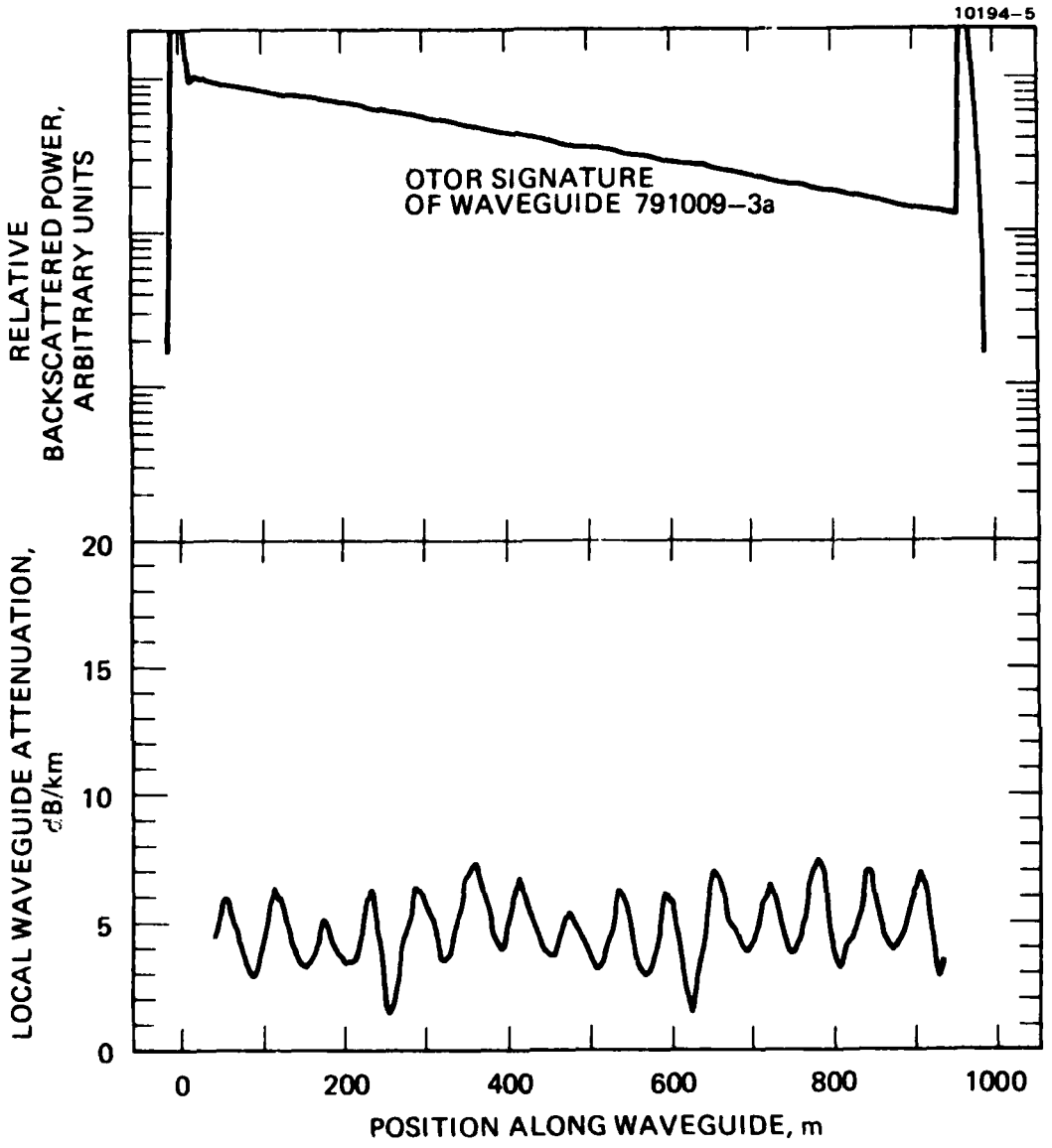

Figure 20. OTDR signature of the ITT fiber.

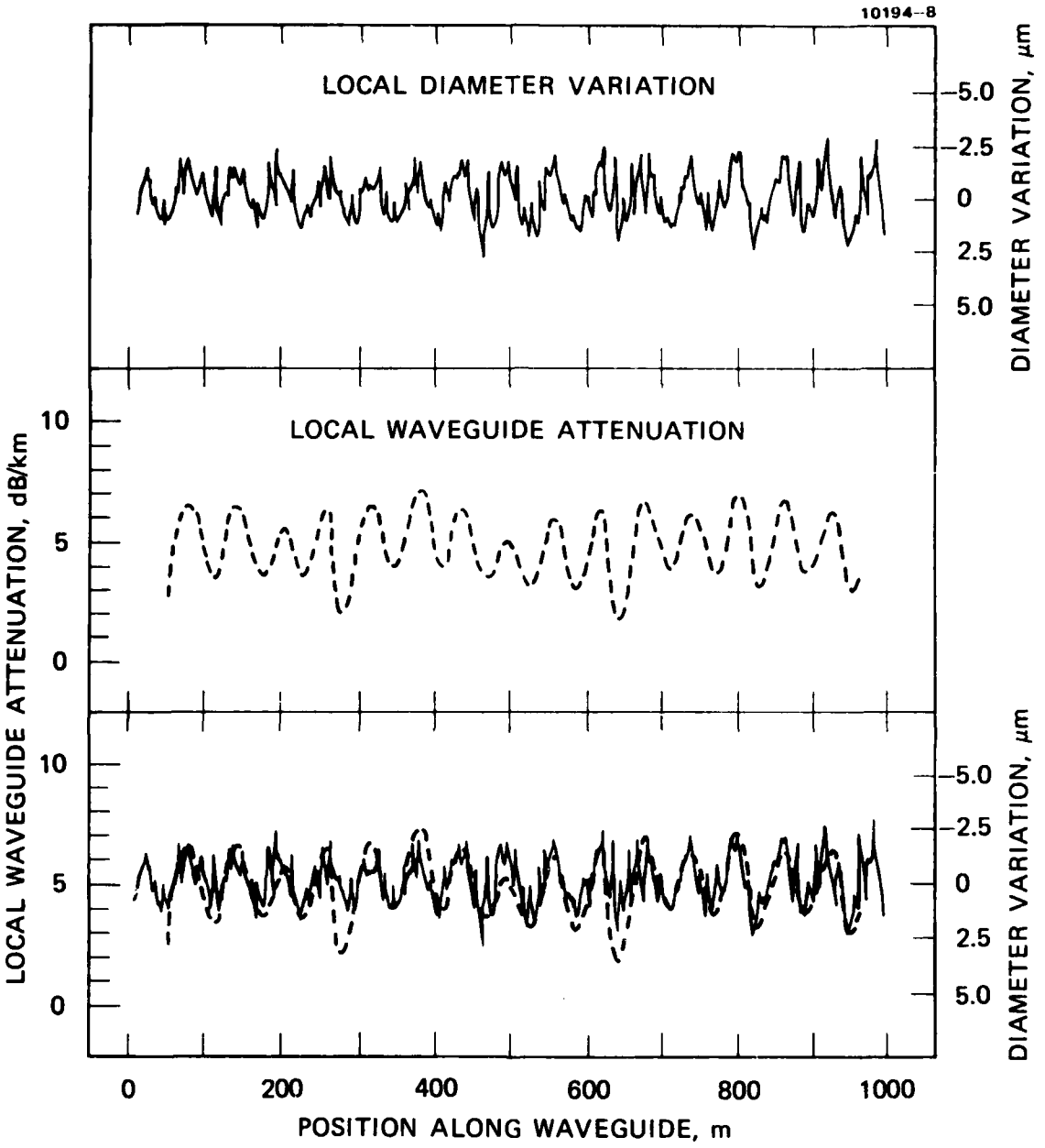

Figure 21. Diameter and signature of the ITT fiber.

To try to improve our understanding of these observations, a special uncoated waveguide was drawn (Figure 22, curve D.) The waveguide has a nominal outer diameter of 126 μm. This diameter was held constant to better than ±1/4 μm for the first 150 m. Then sinusoidal diameter fluctuations of 150 m period and 10 μm amplitude were drawn into the fiber. The silica-germanium-phosphorus core of this step-index fiber has a diameter of 70 μm. The silica-boron buffer layer is 3 μm wide. The clad is 126 μm in diameter and is made from an Hereaus-Amersil T08-WG tube. The NA is 0.20.

The forward OTDR signature is shown in Figure 22, curve P_f. For this characterization, a 50-μm spot, 0.2 NA launch configuration was employed. Thus all mode groups were excited with nearly equal power. The signature is similar to the diameter variation, but there are unexpected complications. First, note that the local peaks in backscattered signal occur when the fiber diameter is minimum as was noted previously. However, there is a shift between the location of the diameter maxima and the local backscattering minima. This shift is equivalent to a 60° phase shift. Note also that the signature looks like the sum of a linear function and a sinusoid. Observation: if linear and sinusoidal functions are added, the peaks of the composite shift in phase with respect to the original sinusoid by $\pm\sin^{-1}$ of the slope of the linear function. Also note that the average slope of this signature is 30°.

Observe that whenever the fiber diameter decreases, the slope of the backscattered return also decreases and can become positive. Normally this would be interpreted as a decrease in the local attenuation. However, if the modes of the fiber are filled at the launch, and if the diameter is reduced, then the number of bound modes are converted to radiation modes and loss is incurred. The conclusion to be reached is that OTDR characterizations of waveguides with large diameter variations must be interpreted carefully.

The waveguide was also characterized from the opposite end (Figure 22, curve P_b). Although the launch conditions are the same, the backscattered signal is different. No longer is there a backscattered maxima when the fiber diameter is a minimum. However, there is a slight bump on the signature which does correspond to diameter minima. Also apparent is the fact that the local backscattering minima are in phase between the two characterizations. The local backscattering maxima are out of phase. The only significant difference

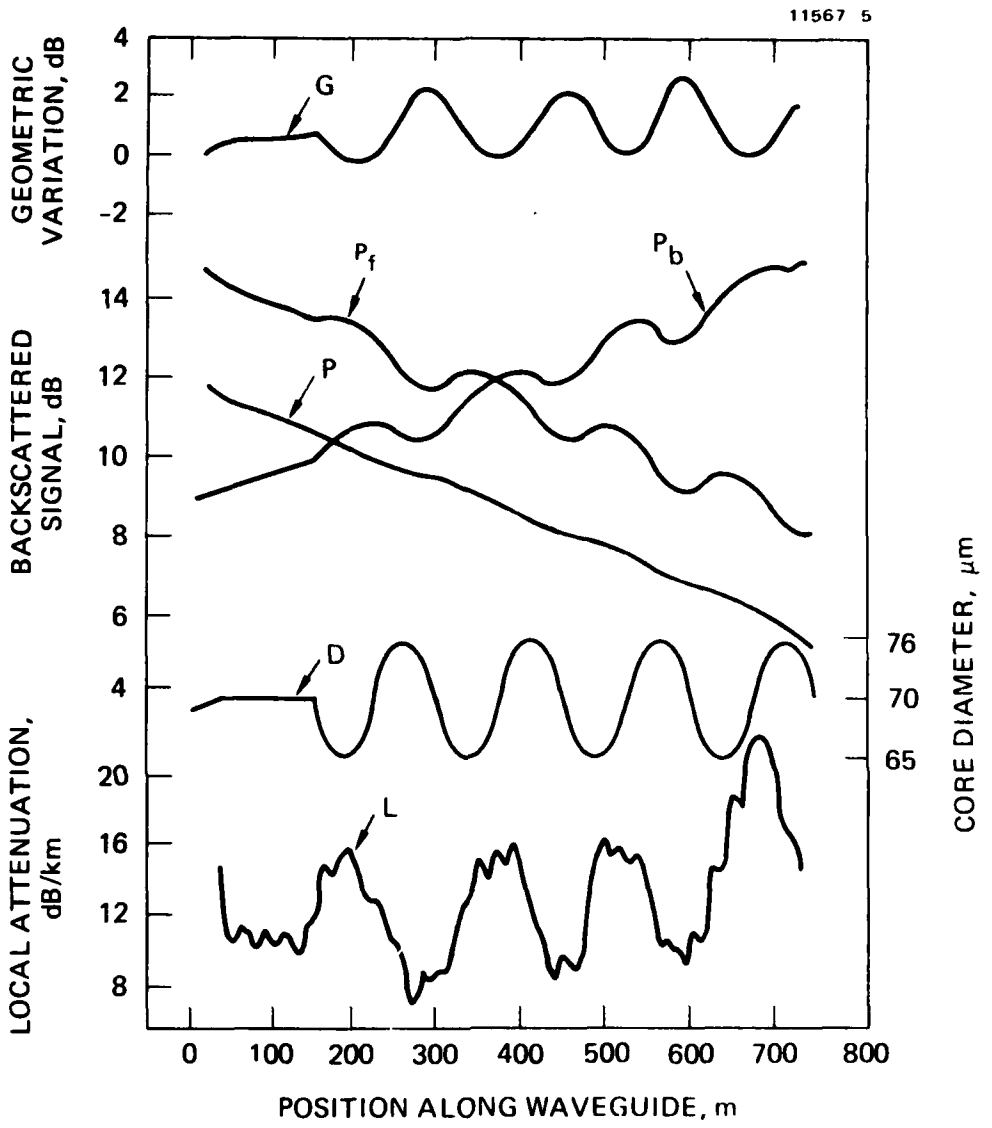

Figure 22. OTDR signature of an experimental fiber with diameter variations.

between these two characterizations is that in the first case the diameter initially decreased, while in this case it initially increases.

DiVita and Rossi[12] developed a method for separating the geometric variation from the power decay (Figure 23). They observed that the backscattered signal consists of two terms: a geometric term and an exponential term. The exponential term contains information about the total attenuation coefficient, α. The geometric term is proportional to the forward scattering and the fiber cross-sectional area. That is, it is proportional to the geometry of the fiber. If the waveguide is characterized from the forward direction, the resulting backscattered signal is given by

$$F = G(z) \exp(\alpha z) \quad . \tag{51}$$

If it is characterized from the backward direction, it is given by

$$B = G(L - z) \exp \{\alpha(L - Z)\} \quad . \tag{52}$$

If the geometric terms are equal, the geometric mean of the forward and backward characterizations is the geometric term, and the square root of the ratio is the exponential term. Thus,

$$G(z) = \sqrt{FB} = \text{constant} \times G(z) \quad ,$$

and

$$P(z) = \sqrt{F/B} = \text{constant} \times \exp(\alpha z) \quad . \tag{53}$$

Figure 22, curve G shows the geometric term, along with the fiber diameter. The geometric term is a reasonably good copy of the diameter variation except for a 60° phase shift.

Figure 22, curve P shows the exponential decay term. Only a small deviation from linearity is apparent. Taking the derivative of this curve provides the local attenuation data shown in Figure 22, curve L. Again, there is good correlation. The local attenuation is maximum when the diameter is minimum as expected; however, the 60° phase shift is once again evident. The small amplitude high frequency oscillations are caused by quantization error in the

10836-1

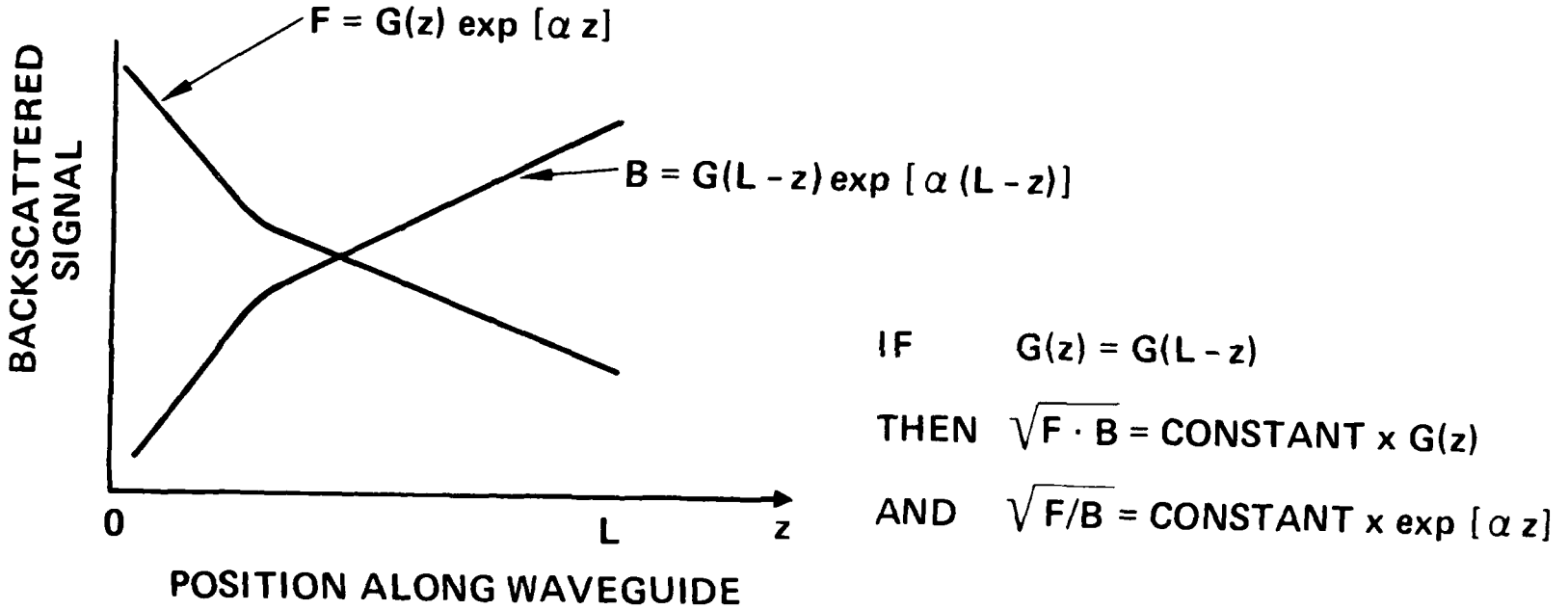

Figure 23. Divita and Rossi separation of power decay and geometry.

transient digitizer. This same experiment was repeated for two other launch modal configurations with identical results. These launch configurations were filling the lowest 1/3 of the mode volume and the highest 1/3.

An independent measurement of the scattered power was also made. The experimental setup is shown in Figure 24. A He-Ne laser beam was chopped and focused onto the core of the waveguide. The launch NA was 0.2. A cladding mode stripper was employed immediately after the launch. Light scattered at right angles to the fiber axis was detected by a PIN photodiode after passing through a 2-mm aperture. A lock-in amplifier measured the detected signal. The waveguide was wound one layer deep on a 30-cm diameter drum. Position along the waveguide was determined by multiplying the meter stick reading by the winding pitch. The experimental results are shown in Figure 25. The average attenuation of the waveguide was 14 dB/km at 0.63 μm. Each data point was corrected to account for this mean attenuation before it was plotted. The scattered power is 180° out of phase with the diameter variations as expected. Power was launched into both ends with qualitatively identical results.

In conclusion, diameter variations can be detected with the OTDR. Features, in general, are not exactly anticorrelated, but exhibit some phase shift. The backscattered signal is complex, but is apparently relatively independent of the launch modal configuration. The sensitivity of the OTDR to diameter variation is about 1.5 dB/km/μm change in core diameter. Diameter changes as small as 1 μm have been detected.

E. PRECISION PERIODIC MICROBEND EXPERIMENT

Microbend transducer is a potential method for tapping power out of optical fibers. The mechanism for bending-induced loss in an optical fiber is the transfer of guided-mode power to the radiation modes. A distortion of spatial periodicity small enough to cause mode conversion is called a microbend. Furthermore, a periodic disturbance of periodicity, Ω, may couple two modes labeled i and j if

$$\frac{2\pi}{\Omega} = \beta_i - \beta_j \equiv \delta\beta_{ij} \quad ,$$

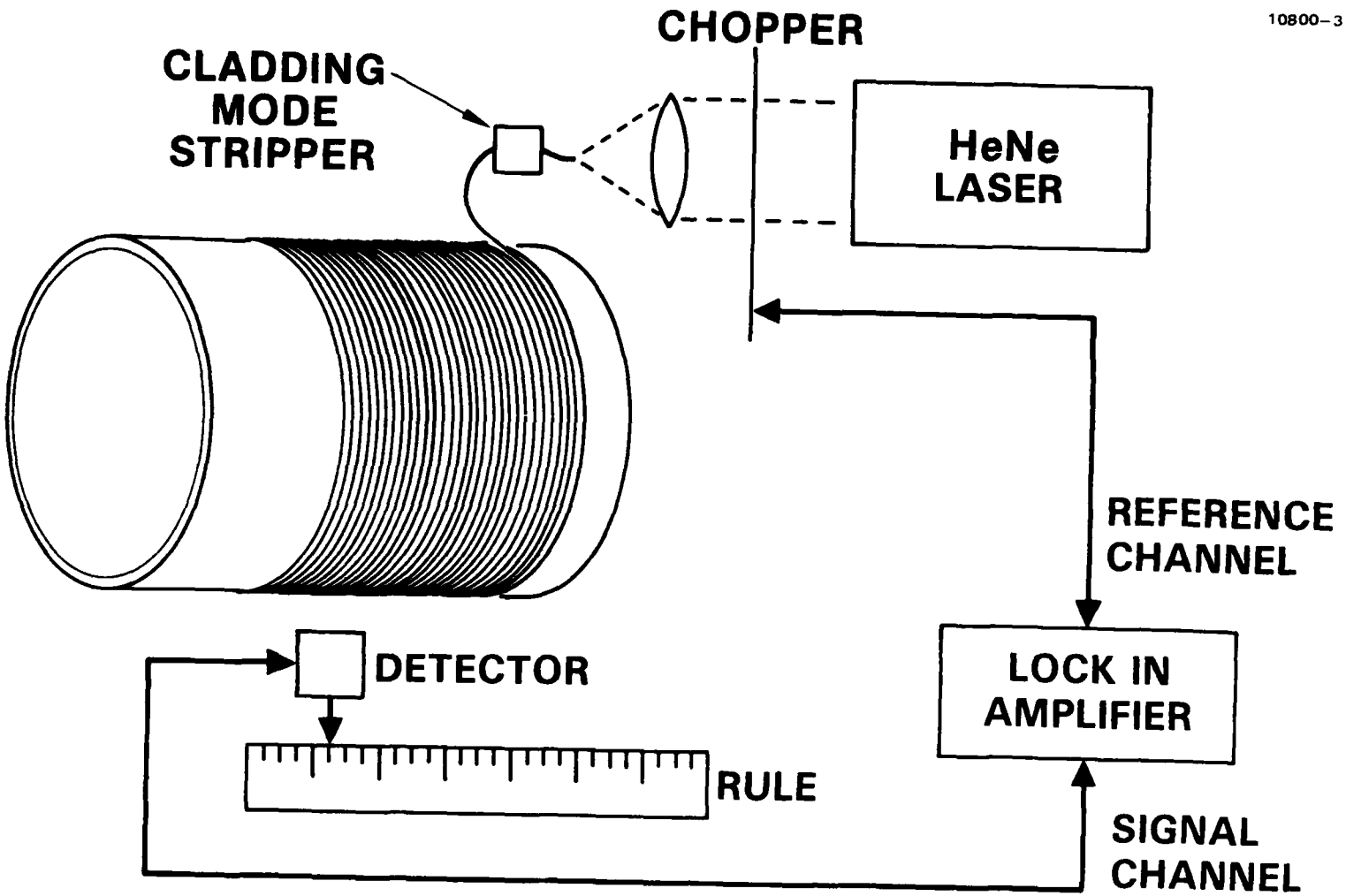

Figure 24. Experimental setup for scattering measurement.

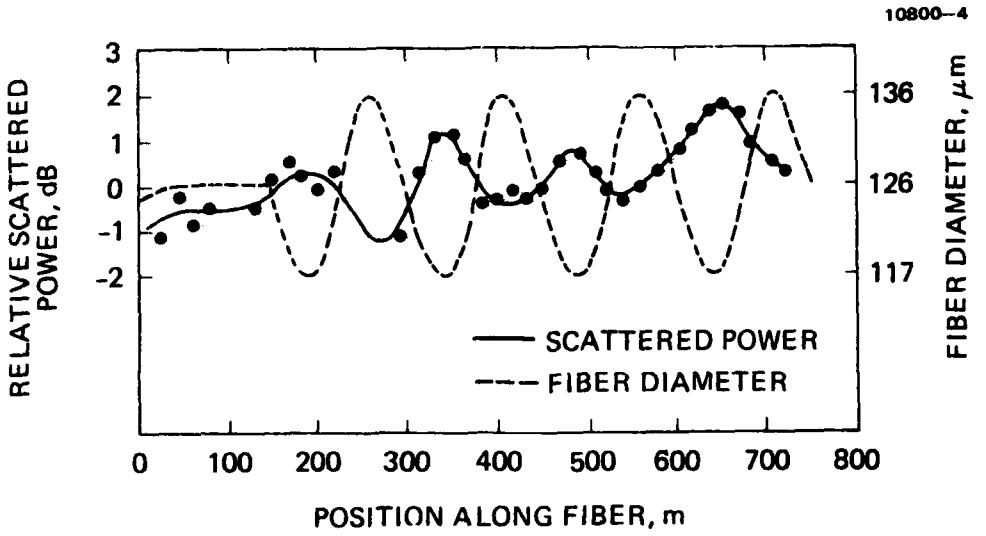

Figure 25. Measured scattering power along the fiber with diameter variation.

where β_i and β_j are the longitudinal propagation constants of modes i and j. Determining those values of Ω that can be expected to cause mode conversion is then reduced to a calculation of $\delta\beta_{ij}$.

For a fiber with the refractive-index profile given by

$$n^2(r) = n_o^2 \left[1 - 2\Delta \left(\frac{r}{a}\right)^\alpha\right] ,$$

r is the radial coordinate, $n_o = n(0)$ is the index at core center, a is the core radius, Δ is the fractional difference in refractive index between cladding and core center, and α is a constant having the value $\alpha = 2$ for a parabolic index fiber and $\alpha = \infty$ for step-index fibers. The longitudinal propagation constants are given by

$$\beta_m = n_o k \left[1 - 2\Delta \left(\frac{m}{M}\right)^{2\alpha/(\alpha+2)}\right]^{1/2} , \tag{56}$$

where $k = 2\pi/\lambda$ (λ is the optical wavelength in vacuum), m is the mode label, and M, the maximum value of m, is

$$M = a n_o k \left(\frac{\alpha\Delta}{\alpha + 2}\right)^{1/2} . \tag{57}$$

The last two equations are valid for highly multimode fibers, and in this limit the total number of modes is equal to M^2.

Defining $\delta\beta_m = \beta_{m+1} - \beta_m$,

$$\delta\beta_m = \frac{2}{a}\left(\frac{\alpha\Delta}{\alpha + 2}\right)^{1/2} \left(\frac{m}{M}\right)^{\alpha-2/\alpha+2} . \tag{58}$$

For a parabolic index fiber ($\alpha = 2$), the last equation yields the interesting result that mode group spacing is independent of mode number:

$$\delta\beta = \frac{(2\Delta)^{1/2}}{a} . \tag{59}$$

The spatial wavelength of interest for mode-coupling considerations is thus

$$\Omega_c = \frac{2\pi}{\delta\beta} = \frac{2\pi a}{(2\Delta)^{1/2}} \quad . \tag{60}$$

For the Corning 1150 graded-index fiber ($2a = 65$ μm and $\Delta = 0.008$), the mode coupling period is $\Omega_c = 1.6$ mm.

For step-index fibers ($\alpha = \infty$), $\delta\beta_m$ becomes

$$\delta\beta_m = \frac{2\Delta^{1/2}}{a}\left(\frac{m}{M}\right) \quad . \tag{61}$$

The largest value of $\delta\beta$ occurs for $m = M$, the smallest value of $\delta\beta$ for $m = 1$:

$$\delta\beta_{max} = \frac{2\Delta^{1/2}}{a} \tag{62}$$

and

$$\delta\beta_{min} = \frac{2\Delta^{1/2}}{a}\,\frac{1}{M} = \frac{2}{n_o ka^2} \quad . \tag{63}$$

For the Corning 1028 step-index fiber ($2a = 85$ μm, $\Delta = 0.008$, $n_o = 1.46$), the corresponding spatial wavelengths are

$$\Omega_{min} = \frac{2\pi}{\delta\beta_{max}} = 1.5 \text{ mm} \quad , \tag{64}$$

and

$$\Omega_{max} = \frac{2\pi}{\delta\beta_{min}} = 8.3 \text{ cm} \quad . \tag{65}$$

From these numerical examples we note that distortions of $\Omega \sim 10$ cm will mix low-lying modes, but smaller Ω's are required to mix the higher order modes. For the parabolic-index fiber, simple bending couples only nearest-neighbor mode groups. Thus only a single Ω is required to cause significant loss. On the other hand, since no simple selection rule exists for the step-index fiber, all wavelengths, $\Omega < \Omega_{min}$, are expected to produce significant loss. No single wavelength will cascade power from low-lying modes of the step fiber to the radiation modes as effectively as does Ω_c for the parabolic fiber.

The preceding analysis leads to an interesting conclusion: if a pure sinusoidal perturbation, with spatial period, $\Omega < \Omega_{min}$, is generated in a step-index fiber, then it is possible to create mode mixing of two specific mode groups without net power loss.

In order to verify this point we carried out the following experiment. The setup is almost identical to that used to measure the insertion loss of a single microbend. The only difference is the microbend transducer is composed of two corrugated plates with precise groove spacings.

A photomask was designed and procured. The pattern contains a periodic array or dark strips 100 μm in width with 1.2 mm period. Two silicon wafers (2 in. diameter) with polished (100) surfaces were sputtered with a SiO_2 film. This, in turn, is used as the mask for the subsequent preferential chemical etching of silicon. A sketch of the profile of the finished silicon wafers is shown in Figure 26. These wafers are mounted on quartz flats, which, in turn, are mounted on vacuum knuckles that allow the two plates to be in perfect parallelism when pressed against each other.

The top plate is stationary while the bottom plate is on a vertical translation stage driven by a digitally controlled stepping motor which has a resolution of ~1 μm.

A spool of multimode step-index fiber ~200 meters long was used in this experiment. The microbend transducer is located about half way along the fiber. Figures 27(a) and (b) shows an OTDR plot of the fiber subject to microbending of various fiber perturbation amplitudes. The fiber sees about 40 periods of microbend. It is seen that a displacement amplitude as small as

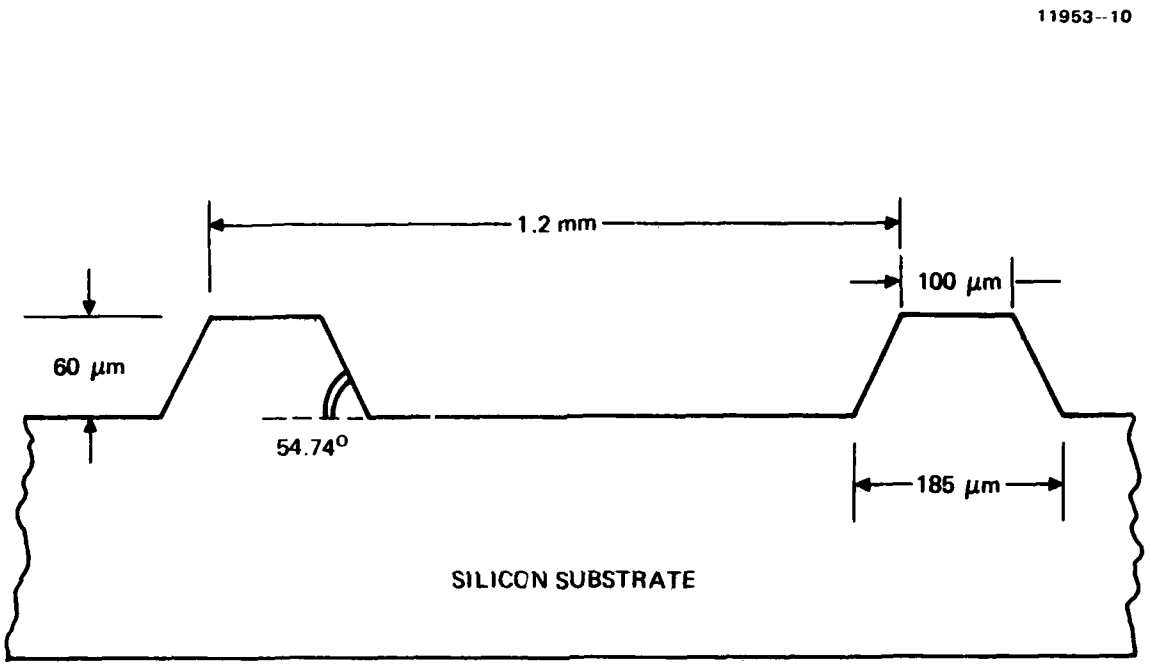

Figure 26. Profile of etched silicon corrugations.

1 μm is detectable on the differential attenuation plot. In this case all modes are launched. We have also selectively launched only lower order modes and only higher order modes. The OTDR plots of these three different cases did not exhibit significant differences as one might expect. We suspect the fiber might not be mode-preserving since it was wound on a small drum without special precautions. Unfortunately, the silicon plates were damaged during one of the runs, precluding further investigations.

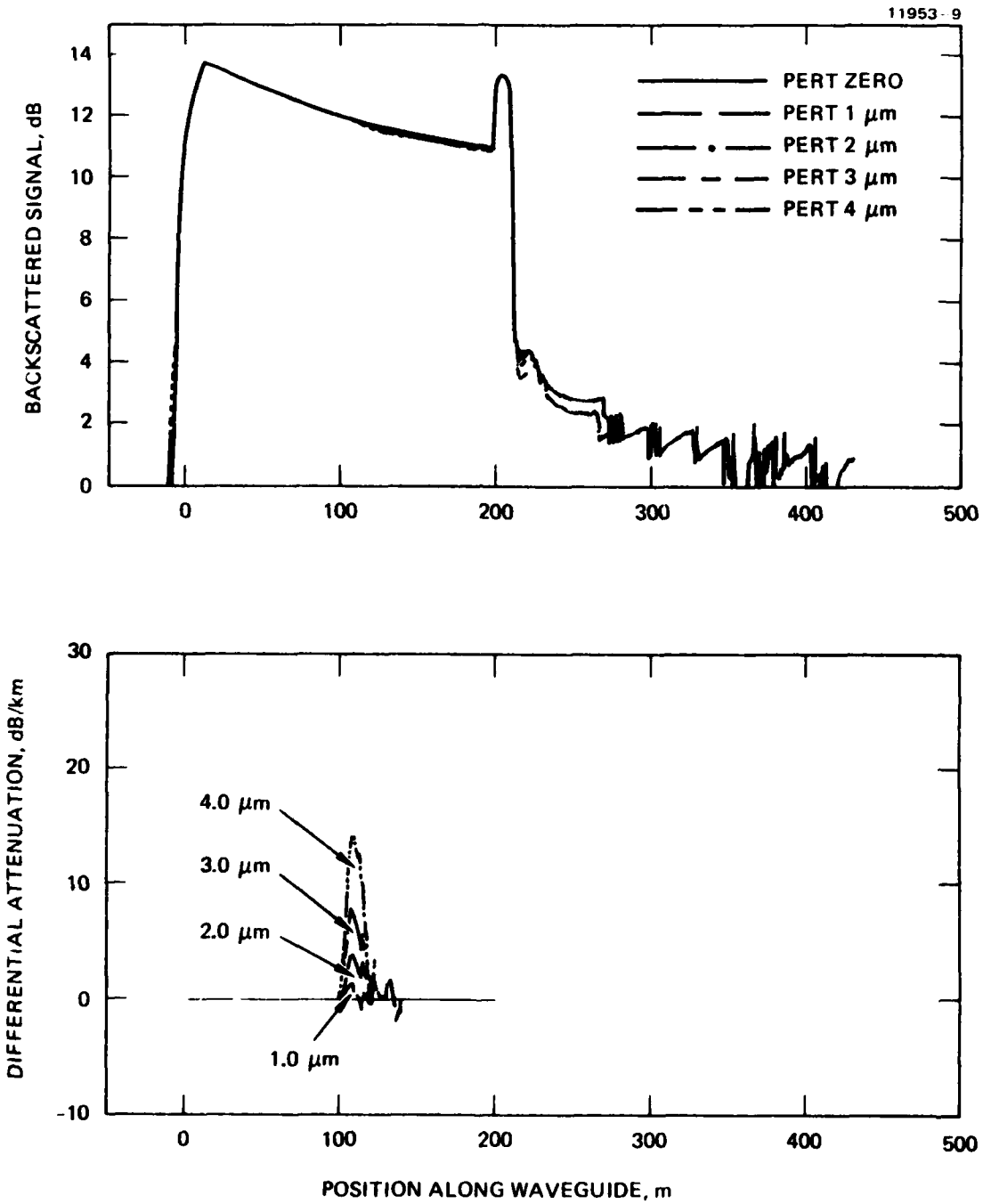

(a) With amplitudes ranging from 1 to 4 μm

Figure 27. OTDR plots of precision periodic microbend.

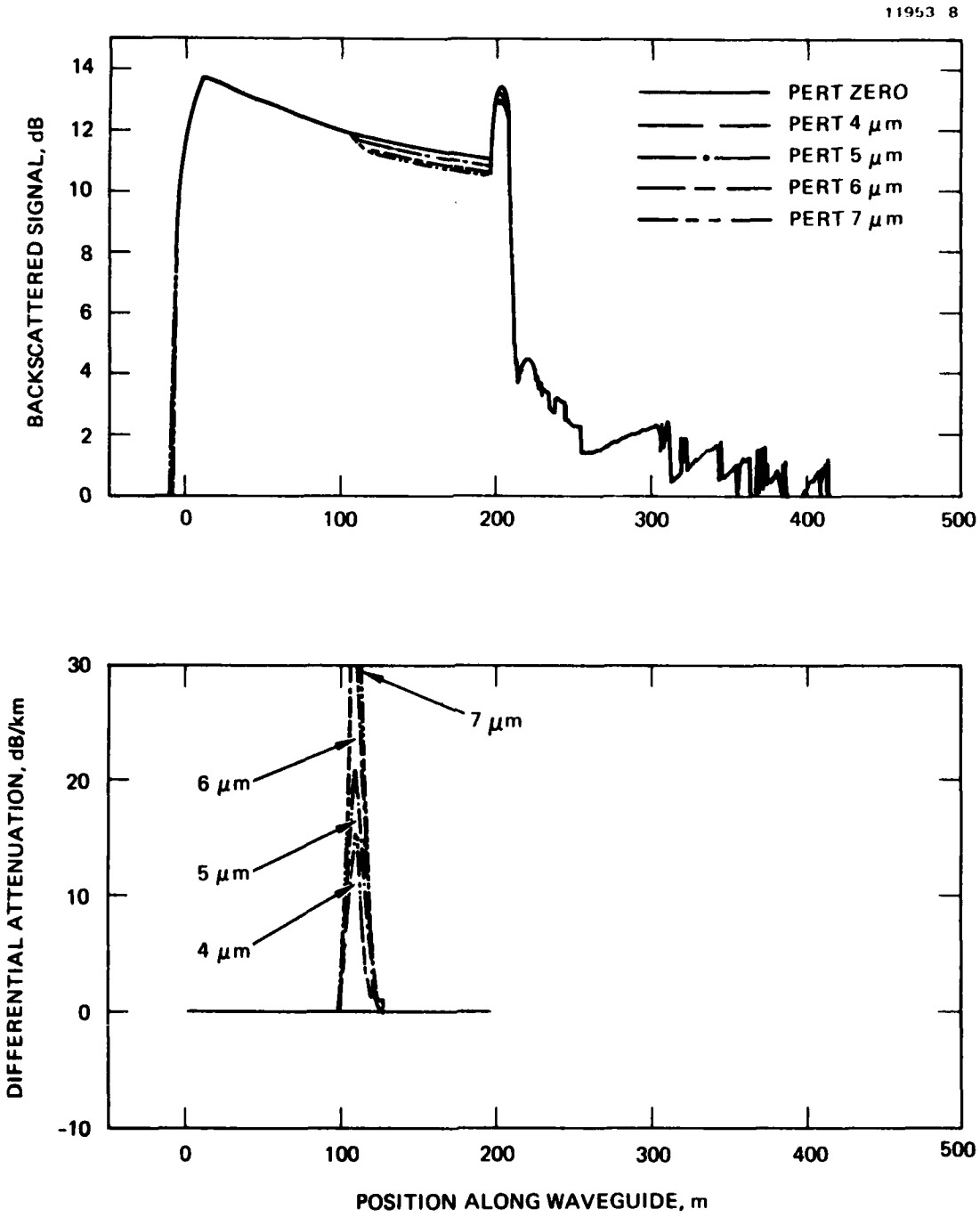

(b) With amplitudes ranging from 4 to 7 μm.

Figure 27. Continued.

SECTION 6

CONCLUSIONS

The OTDR has been shown to be a unique instrument capable of nondestructively performing rapid, accurate, precise measurement of most optical waveguide parameters. It is the only instrument that provides information on the length-dependence of waveguide properties. Total attenuation, scattering loss, absorption loss, location and insertion loss of defects, insertion loss of connectors, splice loss, mode-mixing length, and the effect of environmental perturbations can all be measured. If a waveguide has substantial defects, characterization of the waveguide from both ends allows the spatial variation of waveguide geometry to be separated from the actual power decay.

A series of experiments have been performed which place the OTDR on a firm experimental foundation. Experiments demonstrate that great precision can be achieved in backscatter measurements. The assumption of Rayleigh scattering has been verified. The tremendous power of the OTDR to locate and characterize perturbations has been demonstrated. Diameter fluctuations, microbends, splices and macrobend (e.g., loop) are among the perturbations which have been measured with the instrument.

Theoretical considerations indicated that maximum perturbation sensitivity of the OTDR is achieved by increasing the source power until the threshold for stimulated effects is reached. This maximizes sensitivity regardless of the relative shapes of the probe pulse and the perturbation response. Tailoring the probe pulse shape to be a matched filter for the perturbation results in a further increase in sensitivity at the cost of greatly increased complexity in the source.

Several characteristics of perturbation signatures have been found. Perturbations which are much smaller in spatial extent than the probe pulse are characterized by the shape of the probe pulse. If the probe pulse width is much smaller than the spatial extent of the perturbation, the OTDR response is the impulse response of the perturbation. Fresnel reflection sites can be separated from the Rayleigh scattered signal by reducing the probe pulse width. Reducing the probe pulse width decreases the Rayleigh

scattered signal. Fresnel reflection depends only upon an index discontinuity across a dielectric interface; hence, reducing the probe pulse width does not affect the amplitude of the Fresnel reflection.

Experiments on splices indicate that it is very difficult to splice together two waveguides so perfectly that the OTDR is unable to detect the splice. In every observed case, an insertion loss was measured and conversion of bound mode power to leaky modes was observed.

Experiments on measuring the excess loss of a single fiber loop indicated that the OTDR technique is capable of detecting loops as large as 8-cm in. diameter. Larger diameter loops can be located if the system signal-to-noise ratio is improved.

Large as well as small amplitude microbends in a step-index waveguide can easily be located and measured with the OTDR. The microbend transducer introduces an insertion loss and causes mode conversion to leaky modes. Under this program we have detected the presence of a single microbend less than 10 μm in amplitude and the presence of a periodic microbend (~40 periods) of amplitude less than 2 μm.

Further research is necessary in order to understand the modal dependence of the OTDR perturbation signatures.

REFERENCES

1. M. Rourke, S. Jensen, and M. Barnoski, "Fiber parameter studies with the OTDR," in Fiber Optics Advances in Research and Development, Ed. by B. Bendow and S. Mitra (Plenum Press, 1979), pp. 255-268.

2. D. keck, "Optical fiber waveguides," in Fundamentals of Optical Fiber Communiucations ed. by M. Barnoski (Academic Press, 1976), pp. 29-30.

3. H. Osanai, "Effects of dopants on transmission loss of low-OH-content optical fibers," Elect. Lett. 12, 549 (1976).

4. P. DiVita and U. Rossi, "The backscattering technique: its field of applicability in fiber diagnostics and attenuation measurements," Opt. and Quant. Elec. 11, 17 (1980).

5. R. Olshansky, "Propagation in glass optical waveguides," Rev. Mod. Phys. 51, 341 (1979).

6. M. Barnoski and S. Jensen, "Fiber waveguides: a novel technique for investigating attenuation characteristics," Appl. Opt. 15, 2112 (1976).

7. B. Costa, C. DeBernardi, and B. Sordo, "Investigation of scattering characteristics and accuracy of the backscattering technique by wavelength dependent measurements," 4th European Conference on Optical Communications, Geneva, Sept. 12-15, 1978.

8. M. Born and E. Wolfe, Principles of Optics, 4th Ed. (Pergamon Press, 1970), p. 652.

9. D. Gloge and E. Marcatili, "Multimode theory of graded core fibers," Bell Syst. Tech. J. 52, 1563 (1973).

10. M. Rourke, "Maximum achievable crosstalk isolation in full-duplex, single-strand fiber-optic systems," Opt. Comm. 25, 40 (1978).

11. M.D. Rourke, "An overview of optical time domain reflectometry," Advances in Ceramics, Volume 2, (Physics of Fiber Optics American Ceramic Society, 1981); p. 252.

12. P. DiVita and U. Rossi, "Backscattering measurements in optical fibres: separation of power decay from imperfection contribution," Elect. Lett. 15, 467 (1979).